

THESIS

ELASTICITY-BASED VIBRATIONS OF HOLLOW ANISOTROPIC BEAMS AND AN
EVALUATION OF THE SHAPE FACTOR FOR HOLLOW ANISOTROPIC SECTIONS

Submitted by

Michael J. Lebsack

Department of Civil and Environmental Engineering

In partial fulfillment of the requirements

For the Degree of Master of Science

Colorado State University

Fort Collins, Colorado

Summer 2012

Master's Committee:

Advisor: Paul Heyliger

Marvin Criswell
Christian Puttlitz

ABSTRACT

ELASTICITY-BASED VIBRATIONS OF HOLLOW ANISOTROPIC BEAMS AND AN EVALUATION OF THE SHAPE FACTOR FOR HOLLOW ANISOTROPIC SECTIONS

This study considers the transverse vibrations and natural frequencies of hollow anisotropic beams free from end restraints using full three-dimensional elasticity solutions and common one-dimensional beam theory approximations. Calculations of the natural frequencies are made for a number of hollow beam dimensions using the one-dimensional Euler-Bernoulli, Rayleigh, and Timoshenko beam theories. Complete derivations of the elasticity solutions and beam theories are presented. The accuracy of the approximate methods is determined by comparison to elasticity solutions. Subsequent discussion on the limitations of each approximate beam theory in calculating natural frequencies is made. Mode shapes and cross-section deformations for the first five modes of vibration are presented. Additionally, the shape factor for the Timoshenko beam theory is analyzed for hollow-anisotropic sections.

TABLE OF CONTENTS

Chapter 1: Introduction	1
Chapter 2: Literature Review.....	5
Chapter 3: Theoretical Development.....	10
3.1 Governing Equations	10
3.2 Beam Theories	14
3.2.1 Euler-Bernoulli Beam.....	14
3.2.2 Rayleigh Beam.....	18
3.2.3 Timoshenko Beam	22
3.3 Three-Dimensional Elasticity Solutions	31
3.4 Computations	31
Chapter 4: Results and Discussion.....	33
Chapter 5: Conclusions	65
5.1 Anisotropic Beams.....	65
5.2 Isotropic Beams	67
5.3 Shape Factor.....	70
5.4 Summary	73
References.....	75
Appendix	77

LIST OF TABLES

Table 1. Euler-Bernoulli Wave Numbers	18
Table 2. Undeformed Cross-Sections	40
Table 3. Dimensionless Natural Frequencies--Wall Thickness 0.0005 m (Anisotropic)	41
Table 4. Dimensionless Natural Frequencies--Wall Thickness 0.001 m (Anisotropic)	42
Table 5. Dimensionless Natural Frequencies--Wall Thickness 0.002 m (Anisotropic)	43
Table 6. Dimensionless Natural Frequencies--Wall Thickness 0.004 m (Anisotropic)	44
Table 7. Dimensionless Natural Frequencies--Wall Thickness 0.0005 m (Isotropic)	45
Table 8. Dimensionless Natural Frequencies--Wall Thickness 0.001 m (Isotropic)	46
Table 9. Dimensionless Natural Frequencies--Wall Thickness 0.002 m (Isotropic)	47
Table 10. Dimensionless Natural Frequencies--Wall Thickness 0.004 m (Isotropic)	48
Table 11. Percent Error from Elasticity Solutions (Anisotropic)	49
Table 12. Percent Error from Elasticity Solutions (Isotropic)	50
Table 13. Mode 1 Deformed Cross-Sections	60
Table 14. Mode 2 Deformed Cross-Sections	61
Table 15. Mode 3 Deformed Cross-Sections	62
Table 16. Mode 4 Deformed Cross-Sections	63
Table 17. Mode 5 Deformed Cross-Sections	64
Table 18. Suggested Uses of Beam Theories (Anisotropic)	67
Table 19. Suggested Uses of Beam Theories (Isotropic)	69
Table 20. Percent Error from Elasticity Solutions Using Adjusted Shape Factor	72
Table 21. Shape Factor from Matching Frequencies	73
Table 22. Slenderness Ratios	78

LIST OF FIGURES

Figure 1. Mode 1 Percent Error from Elasticity--Wall Thickness 0.0005 m.....	51
Figure 2. Mode 1 Percent Error from Elasticity--Wall Thickness 0.001 m.....	51
Figure 3. Mode 1 Percent Error from Elasticity--Wall Thickness 0.002 m.....	52
Figure 4. Mode 1 Percent Error from Elasticity--Wall Thickness 0.004 m.....	52
Figure 5. Scaled Mode 1 Frequencies--Wall Thickness 0.0005 m.....	53
Figure 6. Scaled Mode 1 Frequencies--Wall Thickness 0.001 m.....	53
Figure 7. Scaled Mode 1 Frequencies--Wall Thickness 0.002 m.....	54
Figure 8. Scaled Mode 1 Frequencies--Wall Thickness 0.004 m.....	54
Figure 9. Mode 1 Deformation--Length of 0.20 m	55
Figure 10. Mode 2 Deformation--Length of 0.20 m	55
Figure 11. Mode 3 Deformation--Length of 0.20 m	56
Figure 12. Mode 4 Deformation--Length of 0.20 m	56
Figure 13. Mode 5 Deformation--Length of 0.20 m	57
Figure 14. Mode 1 Deformation--Length of 0.05 m	57
Figure 15. Mode 2 Deformation--Length of 0.05 m	58
Figure 16. Mode 3 Deformation--Length of 0.05 m	58
Figure 17. Mode 4 Deformation--Length of 0.05 m	59
Figure 18. Mode 5 Deformation--Length of 0.05 m	59

Chapter 1

Introduction

The topic of vibrating beams has been of interest to engineers for a number of years. The eigenvalue problem provides important information about the interaction between a structure or any finite object and forcing frequencies. The natural frequencies of structures are often examined to determine how those structures will be affected by the frequencies caused by earthquakes and other dynamic loads. Free vibrations are also studied to determine elastic constants of solids small in scale for which traditional experimental methods are not practical [1]. In these resonance methods, an accurate determination of natural frequencies is essential.

The calculation of the natural frequencies of a system is of great significance to engineers of many disciplines. In the design of buildings, bridges, or vehicles, for example, the resonance condition is to be avoided. Resonance occurs when the ratio between the input frequency and the natural frequency of the system approaches unity [2]. The largest amplitudes of motion occur at the resonance frequency. These motions can be potentially destructive to the system. As a result, much care must be taken to ensure the calculations of natural frequencies are accurate. Olhoff and Parbery used an optimization of the difference between subsequent natural frequencies as a way of preventing the resonance condition [3].

Extensive work has been done to study the natural frequencies of isotropic and anisotropic beams, but little has been done to evaluate hollow beams. Four simplifications to the exact

three-dimensional elasticity theory calculations exist, namely the Euler-Bernoulli, Rayleigh, Shear, and Timoshenko beam theories. This paper will discuss the one-dimensional Euler-Bernoulli, Rayleigh, and Timoshenko beam theories and how they compare to Ritz-based approximations to linear theory of elasticity. Discussions will be made on how each of these one-dimensional simplifications to the exact method performs on hollow beams of varying lengths. One-dimensional beam theories only consider the deflection of a beam in one direction, and do not take into account any dilatational or volume changes of the solid. The work of others has shown that with uniform short and stocky beams, one-dimensional beam theories introduce a great deal of error when compared to elasticity solution methods. That is, as the slenderness ratio decreases, the beam theories tend to fail. It is the intent of this paper to determine precisely when it is no longer prudent to use the simplified beam theories. An examination of the first five non-zero natural frequencies will be conducted for a number of hollow beam geometries. Although it is typical to ignore the higher frequencies in design of a structure, especially for relatively short structures, the subsequent frequencies allow for a more complete comparison to elasticity solutions. More error is introduced in the one-dimensional beam theories with the higher order modes. These errors grow more apparent as the slenderness ratio of the beam decreases.

In addition to the evaluation of the natural frequencies of transversely vibrating beams, mode shapes and cross-section deformations of the beam will be examined. The mode shapes can provide a visual picture of how a beam will deform through different frequencies of vibration. The higher modes of vibration are present in all structures, though the first mode shape typically dominates the displacement motion. The higher order mode shapes become more prevalent in

taller structures. Plots of the cross-sectional deformations at varying frequencies and modes of vibration are useful to depict how beams will behave with different wall thicknesses.

A number of boundary condition combinations exist for a beam, however this paper will focus solely on the free-free case for which no shear or moment can be transmitted. For the free-free case, the stress traction vector will equal zero, allowing for a straightforward comparison of each of the beam theories.

Specific consideration is given to hollow sections for two key reasons. First, the use of hollow structural sections in construction is increasing appreciably. The primary reason for this is due to the efficient nature of the hollow section. Hollow sections are lighter than solid sections and their closed shape proves beneficial to the resistance of torsional effects [4]. Secondly, little work has been done to evaluate the transverse vibration of hollow sections. The most notable work was completed by Traill-Nash and Collar over 60 years ago on a built-up box beam section that included diaphragms for buckling reinforcement, but even these authors suggest a more complete study is necessary [5]. Hollow sections have uses outside the realm of structural engineering as well. For example, several components of the aerospace industry can be modeled as a hollow beam, including airplane wings or fuselages [5].

Most engineering materials are classified as anisotropic. For this reason, attention is given to hollow anisotropic sections. The reduction from anisotropic to isotropic is trivial to make. For comparative purposes, the natural frequencies of the isotropic beam have been calculated as well. Composite materials that exhibit anisotropic properties are often used because they present some other benefit to the application of interest. For example, the composite graphite-magnesium is used for its high modulus of elasticity and low density. Aldraihem, Wetherhold, and Singh

performed a comparison of the Euler-Bernoulli and Timoshenko models as they relate to laminated composites [6].

To this point, the only knowledge of a proposed method for determining the shape factor for hollow orthotropic beams is for laminated composites and uses the ratio of the wall thicknesses in its calculations [7]. This procedure does not account for the wall thickness as it compares to the outside dimensions of the beam. An analysis of the validity of this method will be performed.

Chapter 2

Literature Review

The governing equations of motion for the displacement of a solid can be determined with a combination of Newton's laws of motion and a number of elastic relations [8]. As stated previously, there are several methods used in the evaluation of beam vibrations. Each of the beam theories in use focuses on the transverse displacement and the bending effect. Transverse displacement involves particle displacement perpendicular to the longitudinal axis of the beam. Initial work on transversely vibrating beams was performed by Daniel Bernoulli and Leonhard Euler in the 18th century. Daniel Bernoulli is credited with the formulation of the differential equation of motion of a vibrating beam [9]. It was Daniel's uncle Jacob Bernoulli who discovered the relationship between the curvature of a beam and the bending moment. Leonhard Euler is responsible for much of the work regarding the deflected shape of elastic beams under a number of loading conditions.

Together, the formulations made by both Euler and Bernoulli create the first and most basic beam theory. The Euler-Bernoulli beam theory, as it is most commonly known, considers only the bending moment and the lateral displacement. Elishakoff and Pentarus present the Euler-Bernoulli beam in closed form by utilizing a semi-inverse method that specifies the natural frequency [10]. With this method, systems can be designed for a specific natural frequency and mode shape.

In the late 19th century, Lord Rayleigh developed an improvement to the Euler-Bernoulli model with the inclusion of the rotary inertia term. These governing equations became known as Rayleigh's equations [11]. The rotational inertia accounts for the rotation of the cross section in addition to the consideration of the bending moment and lateral displacement.

Stephen Timoshenko took the analysis of transversely vibrating beams one step further with the inclusion of a shear deflection term [11]. The addition of the shear term, and more specifically the shear coefficient or shape factor, has been of particular interest to engineers including the likes of Cowper, Mindlin, and Rubin [12, 13, 14]. The shape factors exist for beams of varying cross-sections. The work of Rubin suggests that a shape factor equal to one is necessary for a variety of reasons [14]. The shape factor for a thin-walled square tube reported by Cowper will be used for the analysis of the hollow isotropic beam sections [12]. Cowper's formulation can be found in the appendix. The shape factor for the hollow anisotropic beams used in this study comes from the work of Puchegger and colleagues regarding anisotropic rectangles [15].

Omidvar develops a shape factor for hollow orthotropic laminated composites, but with the neglecting of the Poisson ratio, this gives the same result as that produced by Cowper [7]. This method also disregards the magnitude of the wall thickness and only considers the ratio of the web and flange thicknesses. Traill-Nash and Collar demonstrate that the effect of the shear term in vibration analysis plays a much larger role in comparison to the rotational inertia term [5].

The exact solution to the problem of the vibrating beam with the use of elasticity solutions was carried out independently by Pochhammer and Chree at the end of the 19th century [9, 16]. The so called Pochhammer-Chree frequency equation has been used by several authors in a number of applications. Benatar, Rittel, and Yarin used a simplification of the Pochhammer-Chree frequency equation in their study of the material and geometric dispersion of viscoelastic

materials [17]. Kolsky examined the effects of dilatational and distortional wave propagation at varying frequencies to understand the effects of dispersion as well [8]. Bancroft used the work completed by Pochhammer and Chree on cylindrical rods to develop a relation between the phase velocity and wave number [18]. Puckett and Peterson used the Pochhammer-Chree solutions to examine wave propagation for multiple modes of vibration [19]. Abramson, Plass, and Ripperger examine both the Pochhammer-Chree solutions and approximate beam theories to evaluate stress wave propagation in beams [20]. In this study, the elasticity solutions first used by Pochhammer and Chree will serve as a benchmark in the comparison of the Euler-Bernoulli, Rayleigh, and Timoshenko beam theories.

Elasticity solutions are inherently more complex than approximate beam theory methods due to the computational nature of the eigenvalue problem. The work of Demarest, Ohno, Visscher, and Heyliger utilizes Hamilton's principle and Ritz-based approximations to solve the problem of the traction free solid that is of interest in this paper [21, 1, 22, 23]. Demarest uses Rayleigh-Ritz approximations in his study of the isotropic cube [21]. Visscher demonstrates that the Hamilton's principle approach can also be applied to a wide array of anisotropic objects [22]. Heyliger and Jilani evaluated the natural frequencies of cylinders and spheres in free vibration using Hamilton's principle and Ritz-based approximations in multiple coordinate systems [23]. Heyliger's unpublished study on the accuracy of the approximate beam theories for solid parallelepipeds serves as the basis for the work of this paper. In this paper, the earlier efforts by Heyliger have been extended into an examination of hollow beam sections that are more commonplace in recent engineering and construction.

The authors Penny and Reed used an integral equation approach as an approximate numerical method to the problem of vibrating beams [24]. However, their work did not consider a beam

free from end restraint. Schmidt used a combination of the Ritz-Rayleigh, Sturm-Liouville, and Stodola-Vianello methods to provide accurate numerical approximations to the fundamental frequencies of a vibrating beam [25]. Elasticity solutions have a number of applications besides the beam. Liew and Yang performed a study regarding three-dimensional elasticity solutions on the free vibrations of circular plates, Love examined the vibrations of cylinders, and Visscher analyzed shapes such as spheres, eggs, cones, and pyramids to name a few [26, 27, 22].

The frequency analysis of the beam problem, including evaluation of mode shapes and frequency equations, has been studied by authors including Traill-Nash and Collar, Dolph, Kruszewski, and Huang [5, 28, 29, 30]. Of particular interest to this paper is the work by Traill-Nash, Collar, Kruszewski, and Huang that involves the free-free boundary condition. Traill-Nash and Collar also provide an explanation of how the rotary inertia term in hollow beam sections is even less important than for solid sections. Traill-Nash and Collar used closely spaced diaphragms to reinforce the hollow section to limit the effects of buckling and to give the beam a mass loading to reduce the natural frequencies so that they could be measured experimentally [5]. In this present study, no transverse diaphragms will be used, in part because physical testing is not considered. Kruszewski performed a study on the free vibrations of box beams as well. His work used the same Rayleigh-Ritz method of approximations as discussed earlier, but focused on the torsional vibrations as opposed to transverse vibrations that will be discussed in this paper. Kruszewski concluded that the cross-sectional deformation due to shear effects is important to consider for beams with fewer bulkheads [29]. The bulkheads that are used in the hulls of ships or airplane wings and fuselages are very similar in nature to the transverse diaphragms used by Traill-Nash and Collar. Thompson and Kruszewski performed an analysis on thin wings with an airfoil-type cross-section that also considered the importance of cross-sectional deformations on

the natural frequencies [31]. In their analysis, the airfoil shaped wing was modeled as two curved beams. Huang provides excellent derivations of the frequency equations for flexural vibrations for a number of end restraint combinations, including the free-free case [30].

Chapter 3

Theoretical Development

Section 3.1: Governing Equations

The governing equations of motion and the frequency equations can be determined with the use of Newton's laws and the elastic relations of solids. The evaluation of natural frequencies is simplified by the condition of traction free surfaces. The free-free boundary condition also allows for a more direct comparison between beam theories and elasticity methods. By assuming that the solid is linear elastic, Hooke's law is used to relate the components of the infinitesimal or Cauchy strain tensor to the elastic stiffness tensor. It states that stress varies as the stretch

$$\sigma_{ij} = C_{ijkl} \epsilon_{kl} \quad Eq (1)$$

where σ_{ij} represents the second-order elastic stress tensor, C_{ijkl} is the fourth-order elastic stiffness tensor, and ϵ_{kl} represents the second-order Cauchy strain tensor. This law represents nine equations. However, if the material is isotropic, symmetry is introduced and the system can be reduced significantly. When strains are infinitesimal, the Cauchy strain tensor can be represented by the strain-displacement equation below

$$\epsilon_{ij} = \frac{1}{2} (u_{i,j} + u_{j,i}) \quad Eq (2)$$

where $u_{i,j}$ and $u_{j,i}$ are partial derivatives of the transverse displacement with respect to the orthogonal coordinate direction.

Fung and Tong present a derivation of the equations of motion similar to that described below [11]. For an oscillating solid that undergoes small deformations, the equation of motion is given as

$$\sigma_{ij,j} + f_i = \rho \frac{\partial^2 u_i}{\partial t^2} \quad Eq (3)$$

where f_i represents the body force vector and ρ is the mass density of the solid. The virtual work done by the body force vector and the surface traction vector is given as

$$\int_V f_i \delta u_i dV + \int_S T_i^n \delta u_i dS$$

where δu_i represents the virtual displacements and T_i^n represents the surface traction vector.

Using Cauchy's formula that states

$$T_i^n = \sigma_{ij} n_j, \quad Eq (4)$$

the virtual work of the surface traction vector becomes

$$\int_S T_i^n \delta u_i dS = \int_V \sigma_{ij,j} \delta u_i dV + \int_V \sigma_{ij} \delta \epsilon_{ij} dV. \quad Eq (5)$$

Now, utilizing Eq (3) and the symmetry of stress, the right hand side of Eq (5) becomes

$$\int_V \left(\rho \frac{\partial^2 u_i}{\partial t^2} - f_i \right) \delta u_i dV + \int_V \sigma_{ij} \delta \epsilon_{ij} dV.$$

Finally, the variational equation of motion is given as

$$\int_V \sigma_{ij} \delta \epsilon_{ij} dV = \int_V f_i - \rho \frac{\partial^2 u_i}{\partial t^2} \delta u_i dV + \int_S T_i^n \delta u_i dS \quad Eq (6)$$

Assuming that the solid is elastic, a substitution of the strain energy density can be made into the variational equation of motion as follows

$$\delta \int_V W dV = \int_V f_i - \rho \frac{\partial^2 u_i}{\partial t^2} \delta u_i dV + \int_S T_i^n \delta u_i dS \quad Eq (7)$$

where W represents the strain energy density. By letting the virtual displacements δu_i be functions of space and time, the variational equation of motion can be integrated with respect to time to yield another variational principle

$$\int_{t_0}^{t_1} \int_V \delta W dV = \int_{t_0}^{t_1} \int_V f_i \delta u_i dV + \int_{t_0}^{t_1} \int_S T_i^n \delta u_i dS - \int_{t_0}^{t_1} \int_V \rho \frac{\partial^2 u_i}{\partial t^2} \delta u_i dV. \quad Eq (9)$$

After a few manipulations, the final term in $Eq (9)$ becomes

$$- \int_{t_0}^{t_1} \delta KE dt$$

where KE represents the kinetic energy of the moving solid and

$$KE = \frac{1}{2} \int_V \rho \frac{\partial^2 u_i}{\partial t^2} dV. \quad Eq (10)$$

If the assumption is made that all of the virtual displacements are zero along the beam at the time t_0 and t_1 ,

$$\delta u_i|_{t_0} = \delta u_i|_{t_1} = 0 \quad Eq (11)$$

then $Eq (9)$ becomes

$$\int_{t_0}^{t_1} \int_V \delta(W - KE) dV = \int_{t_0}^{t_1} \int_V f_i \delta u_i dV + \int_{t_0}^{t_1} \int_S T_i^n \delta u_i dS \quad Eq (12)$$

where the right hand side of this equation represents the potential energy of the system due to any external forces acting on the beam. By letting

$$-PE = \int_V f_i \delta u_i dV + \int_S T_i^n \delta u_i dS \quad Eq (13)$$

and

$$U = \int_V W dV \quad Eq (14)$$

where U is the strain energy of the body and PE is the potential energy, we arrive at the extended Hamilton's principle

$$\delta \int_{t_0}^{t_1} (U - KE + PE) dt = 0. \quad Eq (15)$$

Hamilton's principle, named after Sir William Rowan Hamilton, is an integral statement used as the key building block to the equations of motion of dynamic bodies [2]. The transverse vibration of beams is a common application of Hamilton's principle. To apply Hamilton's principle to the problem of the beam, the strain energy, kinetic energy, and potential energy terms in Eq (15) must be known for beam bending. These quantities will differ for the Euler-Bernoulli, Rayleigh, and Timoshenko models.

Section 3.2: Beam Theories

Three-dimensional elasticity solutions to beam bending are very complex problems.

Subsequently, simplifications to the elasticity theory are made that restrict the motion of the solid. By kinematically constraining the deformation of the solid to one dimension using an assumed displacement field, the evaluation of the beam bending can be simplified dramatically.

It is the variations in the assumed displacement fields that make up the one-dimensional beam theories.

Section 3.2.1: Euler-Bernoulli Beam

The Euler-Bernoulli beam theory assumes the simplest and most basic deformation of the beam.

It only considers the transverse displacement of the beam. Neglecting the Poisson effect

assumes that the cross-section of the solid does not change and allows for the reduction to one-dimension. The displacement field of the Euler-Bernoulli Beam is given by

$$u_{x,y,z} = -z \frac{dw}{dx} \quad Eq (16)$$

$$v_{x,y,z} = 0 \quad Eq (17)$$

$$w_{x,y,z} = w(x) \quad Eq (18)$$

where u , v , and w represent the displacement in the x , y , and z directions, respectively. The transverse displacement is represented by the variable w . The process of deriving the frequency equations for the Euler-Bernoulli beam follows closely the work of Han and Fung [9, 11]. Using the displacement field, the strain energy for the Euler-Bernoulli model is given as

$$U = \frac{1}{2} \int_0^L EI \left(\frac{\partial^2 w}{\partial x^2} \right)^2 dx \quad Eq (19)$$

where E represents the modulus of elasticity and I represents the area moment of inertia of the beam. The kinetic energy is given as

$$KE = \frac{1}{2} \int_0^L m \left(\frac{\partial w}{\partial t} \right)^2 dx \quad Eq (20)$$

where m represents the mass per unit length of the beam. For the case of a free-free beam, the surface traction vectors are equal to zero and there are no applied body forces, therefore PE disappears from $Eq (15)$. Substituting into Hamilton's principle yields the following

$$\delta \int_{t_0}^{t_1} \int_0^L \left[\frac{1}{2} EI \left(\frac{\partial^2 w}{\partial x^2} \right)^2 - \frac{1}{2} m \left(\frac{\partial w}{\partial t} \right)^2 \right] dx dt = 0. \quad Eq (21)$$

Using the notion that δw is zero at times t_0 and t_1 , further manipulation gives

$$\int_{t_0}^{t_1} \int_0^L \left[EI \frac{\partial^2 w}{\partial x^2} \frac{\partial^2 \delta w}{\partial x^2} - m \frac{\partial w}{\partial t} \frac{\partial \delta w}{\partial t} \right] dx dt = 0. \quad Eq (22)$$

Performing two steps of integration by parts gives

$$\begin{aligned} & \int_{t_0}^{t_1} \int_0^L \left[\frac{\partial^2}{\partial x^2} \left(EI \frac{\partial^2 w}{\partial x^2} \right) + m \frac{\partial^2 w}{\partial t^2} \right] \delta w dx dt \\ & + \int_{t_0}^t \left[EI \frac{\partial^2 w}{\partial x^2} \delta \frac{\partial w}{\partial x} \right]_0^L dt - \int_{t_0}^t \left[\frac{\partial}{\partial x} \left(EI \frac{\partial^2 w}{\partial x^2} \right) \delta w \right]_0^L dt = 0. \end{aligned} \quad Eq (23)$$

Finally, the equation of motion for the Euler-Bernoulli model is

$$\frac{\partial^2}{\partial x^2} \left(EI \frac{\partial^2 w}{\partial x^2} \right) + m \frac{\partial^2 w}{\partial t^2} = 0. \quad Eq (24)$$

This equation is known as the Euler equation of motion. The boundary conditions to be satisfied for a beam free from end restraint are as follows

$$EI \frac{\partial^2 w}{\partial x^2} \delta \frac{\partial w}{\partial x} \Big|_0^L = 0 \text{ and } \frac{\partial}{\partial x} \left(EI \frac{\partial^2 w}{\partial x^2} \delta w \right) \Big|_0^L = 0 \quad \text{Eqs (25, 26)}$$

where δw is the displacement, $\frac{\partial w}{\partial x}$ is the slope, $EI \frac{\partial^2 w}{\partial x^2}$ is the moment, and $\frac{\partial}{\partial x} \left(EI \frac{\partial^2 w}{\partial x^2} \right)$ is the shear. For the case of the free-free beam, the moment and shear must equal zero to meet the physical limitations of a beam free from end restraint. That is

$$EI \frac{\partial^2 w}{\partial x^2} = 0 \quad \text{Eq (27)}$$

$$\frac{\partial}{\partial x} \left(EI \frac{\partial^2 w}{\partial x^2} \right) = 0. \quad \text{Eq (28)}$$

With the use of separation of variables techniques as laid out by Han [9], where the transverse displacement $w(x, t)$ is

$$w(x, t) = W(x) T(t), \quad \text{Eq (29)}$$

the Euler equation of motion can be split into two ordinary differential equations

$$\frac{d^2 T(t)}{dt^2} + \omega^2 T(t) = 0 \text{ and } \frac{d^4 W(x)}{dx^4} - a^4 W(x) = 0 \quad \text{Eqs (30, 31)}$$

where the wave number a and the angular frequency ω are related as follows

$$a^4 = \omega^2 \frac{\rho A L^4}{EI}. \quad \text{Eq (32)}$$

In frequency analysis it is often convenient to use dimensionless variables. By non-dimensionalizing ω , ρ , A , L , and I as listed in the appendix, the dimensionless wave number can be related to the angular frequency as follows

$$a^4 = \rho^* A^* \omega^{*2}. \quad Eq (33)$$

Here, the variables with the superscript * represent the dimensionless quantities. For the remainder of this study, variables will be presented that include the dimensions so as to aide in future computations unless otherwise noted. The dimensionless wave number is also given as 2π divided by the wavelength. Solving the two ordinary differential equations leads to the solutions

$$T t = D_1 \sin \omega t + D_2 \cos \omega t \quad Eq (34)$$

$$W x = C_1 \sin ax + C_2 \cos ax + C_3 \sinh ax + C_4 \cosh ax \quad Eq (35)$$

with D_1 and C_1 representing arbitrary constants. Rewriting the boundary conditions given in *Eqs (27, 28)* leads to

$$EI \frac{\partial^2 W(x)}{\partial x^2} = 0 \quad Eq (36)$$

$$\frac{\partial}{\partial x} EI \frac{\partial^2 W(x)}{\partial x^2} = 0. \quad Eq (37)$$

From this point, the eigenvalue problem is solved in order to obtain an expression for finding the dimensionless wave numbers.

$$\cos a \cosh a - 1 = 0 \quad Eq (38)$$

By solving for the roots of this equation, the wave numbers for the first five modes of vibration were attained as listed in Table 1 for the case of the free-free beam. The equation for determining the natural frequencies comes from rearranging the dispersion relationship in Eq (32) as follows

$$\omega = \sqrt{\frac{EI}{\rho AL^4}} a^2. \quad \text{Eq (39)}$$

Substituting the wave numbers into Eq (39) will yield the natural frequencies to be discussed later.

Table 1. Euler-Bernoulli Wave Numbers

Wave Numbers				
a_1	a_2	a_3	a_4	a_5
4.730	7.853	10.996	14.137	17.279

Section 3.2.2: Rayleigh Beam

The Rayleigh beam theory builds off of the Euler-Bernoulli theory by accounting for the rotary inertia of the solid. The assumed displacement field of the beam is the same as for the Euler-Bernoulli model, but an additional term will be included in the calculation of the kinetic energy. Again, literature from Han and Fung is followed in the determination of the frequency equations for the Rayleigh beam [9, 11]. The rotation of the beam cross-section is given as

$$\frac{1}{2} \int_0^L \rho I \frac{\partial^2 w}{\partial x \partial t}^2 dx.$$

Now the total kinetic energy is

$$KE = \frac{1}{2} \int_0^L m \frac{\partial w}{\partial t}^2 dx + \frac{1}{2} \int_0^L \rho I \frac{\partial^2 w}{\partial x \partial t}^2 dx. \quad Eq (40)$$

Substituting the strain energy term as given in Eq (19) and the kinetic energy term in Eq (40) into Hamilton's principle of Eq (15) gives

$$\delta \int_{t_0}^{t_1} \int_0^L \left[\frac{1}{2} EI \frac{\partial^2 w}{\partial x^2}^2 - \frac{1}{2} m \frac{\partial w}{\partial t}^2 - \frac{1}{2} \rho I \frac{\partial^2 w}{\partial x \partial t}^2 \right] dx dt = 0 \quad Eq (41)$$

and

$$\int_{t_0}^{t_1} \int_0^L \left[EI \frac{\partial^2 w}{\partial x^2} \frac{\partial^2 \delta w}{\partial x^2} - m \frac{\partial w}{\partial t} \frac{\partial \delta w}{\partial t} - \rho I \frac{\partial^2 w}{\partial x \partial t} \frac{\partial^2 \delta w}{\partial x \partial t} \right] dx dt = 0 \quad Eq (42)$$

when the virtual displacements vanish at times t_0 and t_1 . Integrating by parts twice gives

$$\begin{aligned} & \int_{t_0}^{t_1} \int_0^L \left[\frac{\partial^2}{\partial x^2} EI \frac{\partial^2 w}{\partial x^2} + m \frac{\partial^2 w}{\partial t^2} - \frac{\partial^2 w}{\partial x \partial t} \rho I \frac{\partial^2 w}{\partial x \partial t} \right] \delta w dx dt + \int_{t_0}^t EI \frac{\partial^2 w}{\partial x^2} \delta \left[\frac{\partial w}{\partial x} \right]_0^L dt \\ & - \int_{t_0}^t \frac{\partial}{\partial x} \left[EI \frac{\partial^2 w}{\partial x^2} - \rho I \frac{\partial^2 w}{\partial x \partial t} \right] \delta w \Big|_0^L dt = 0. \end{aligned} \quad Eq (43)$$

The Euler equation of motion now becomes

$$\frac{\partial^2}{\partial x^2} EI \frac{\partial^2 w}{\partial x^2} + m \frac{\partial^2 w}{\partial t^2} - \frac{\partial^2 w}{\partial x \partial t} \rho I \frac{\partial^2 w}{\partial x \partial t} = 0 \quad Eq (44)$$

for a beam free from body forces and surface tractions. The boundary conditions given now become

$$EI \frac{\partial^2 w}{\partial x^2} = 0 \quad Eq (45)$$

$$\frac{\partial}{\partial x} \left[EI \frac{\partial^2 w}{\partial x^2} - \rho I \frac{\partial^2 w}{\partial x \partial t} \right] = 0 \quad Eq (46)$$

for the free-free beam. Using the same separation of variables method with the transverse displacement $w(x, t)$ the same as in Eq (29) again leads to two ordinary differential equations. The differential equation involving $T(t)$ remains the same as Eq 30, and that with $W(x)$ becomes

$$\frac{d^4 W(x)}{dx^4} - a^4 W(x) + \omega^2 \rho I \frac{d^2 W(x)}{dx^2} = 0. \quad \text{Eq (47)}$$

The solutions to these two differential equations are

$$T(t) = D_1 \sin \omega t + D_2 \cos \omega t \quad \text{Eq (48)}$$

$$W(x) = C_1 \sin ax + C_2 \cos ax + C_3 \sinh bx + C_4 \cosh bx \quad \text{Eq (49)}$$

with b as an additional wave number. If the variables are non-dimensionalized once again, the dispersion relationships for the two wave numbers can be presented as

$$a = \frac{\omega^2 \rho^* I^*}{2} + \sqrt{\frac{\omega^2 \rho^* I^*{}^2}{2} + \omega^2 \rho^* A^*} \quad \text{Eq (50)}$$

$$b = \frac{-\omega^2 \rho^* I^*}{2} + \sqrt{\frac{\omega^2 \rho^* I^*{}^2}{2} + \omega^2 \rho^* A^*}. \quad \text{Eq (51)}$$

The boundary conditions in terms of the spatial solution $W(x)$ become

$$EI \frac{\partial^2 W(x)}{\partial x^2} = 0 \quad \text{Eq (52)}$$

$$\frac{\partial}{\partial x} \left(EI \frac{\partial^2 W(x)}{\partial x^2} \right) - \frac{\partial}{\partial t} \left(\rho I \frac{\partial^2 W(x)}{\partial x \partial t} \right) = 0. \quad \text{Eq (53)}$$

As was the case with the Euler-Bernoulli model, the wave numbers are needed in order to obtain the natural frequencies of vibration. Initially the two wave numbers must be expressed in terms of one another. An excellent description of this process is given in the literature of Han [9], which gives

$$B_1 = \frac{\omega^2 \rho^* I^*}{2} \quad \text{and} \quad B_2 = \omega^2 \rho^* A^* \quad \text{Eqs (54, 55)}$$

$$B_1 = \frac{a^2 - b^2}{2} \quad \text{and} \quad B_2 = a^2 b^2. \quad \text{Eqs (56, 57)}$$

This leads to

$$b = a \frac{1}{a^2 k'^2 + 1} = as \frac{1}{a^2 + s^2} \quad \text{Eq (58)}$$

where

$$k' = \frac{I}{A} \quad \text{and} \quad s = L \frac{A}{I}. \quad \text{Eqs (59, 60)}$$

The variable k' is commonly referred to as the radius of gyration and s is the slenderness ratio.

Now the eigenvalue problem is solved for the case of the free-free beam which yields the following expression for attaining the wave numbers

$$b^6 - a^6 \sin a \sinh b + 2a^3 b^3 \cos a \cosh b - 2a^3 b^3 = 0. \quad \text{Eq (61)}$$

This expression contains both wave numbers which are related by the slenderness ratio.

Therefore, to solve for the wave numbers to be used in determining the natural frequencies, specific properties pertaining to the shape of the beam must be known. For the Euler-Bernoulli model, the wave number was independent of the beam geometry and the respective wave

numbers for each mode of vibration do not change. Accordingly, no specific wave numbers can be given for the Rayleigh model. To solve for the natural frequencies, Eqs 54 – 57 are used to give

$$\omega = \sqrt{a^2 - b^2} \frac{E}{\rho L^2}. \quad \text{Eq (62)}$$

Section 3.2.3: Timoshenko Beam

The Timoshenko beam includes the effects of shear along with the transverse displacement and the rotary inertia. The assumed displacement field of the Timoshenko beam is given as

$$u(x, y, z) = z\psi(x) \quad \text{Eq (63)}$$

$$v(x, y, z) = 0 \quad \text{Eq (64)}$$

$$w(x, y, z) = w(x) \quad \text{Eq (65)}$$

where $\psi(x)$ represents the section rotation of the solid. The addition of the shear and rotary inertia terms in the Timoshenko model effectively reduces the stiffness of the solid to better approximate three-dimensional elasticity solutions. Literature from Han and Fung is utilized once more in the Timoshenko theory derivations [9, 11]. Using the displacement field to obtain the normal stresses and normal strains of the Timoshenko model, the strain energy term due to bending becomes

$$U_b = \frac{1}{2} \int_0^L EI \left(\frac{\partial \psi}{\partial x} \right)^2 dx. \quad \text{Eq (66)}$$

Relating the shear strains and shear stresses gives the strain energy due to shear

$$U_s = \frac{1}{2} \int_0^L kGA \left(\frac{\partial w}{\partial x} - \psi \right)^2 dx \quad \text{Eq (67)}$$

where k is introduced as the Timoshenko shear coefficient, also known as the shape factor, and G is the shear modulus of elasticity. The kinetic energy for the Timoshenko model is

$$KE = \frac{1}{2} \int_0^L m \left(\frac{\partial w}{\partial t} \right)^2 dx + \frac{1}{2} \int_0^L \rho I \left(\frac{\partial \psi}{\partial t} \right)^2 dx. \quad \text{Eq (68)}$$

Substituting into Hamilton's principle yields

$$\delta \int_{t_0}^{t_1} \int_0^L \left[\frac{1}{2} EI \left(\frac{\partial \psi}{\partial x} \right)^2 + \frac{1}{2} kGA \left(\frac{\partial w}{\partial x} - \psi \right)^2 - \frac{1}{2} m \left(\frac{\partial w}{\partial t} \right)^2 - \frac{1}{2} \rho I \left(\frac{\partial \psi}{\partial t} \right)^2 \right] dx dt = 0 \quad \text{Eq (69)}$$

and

$$\int_{t_0}^{t_1} \int_0^L \left[EI \frac{\partial \psi}{\partial x} \frac{\partial \delta \psi}{\partial x} + kGA \left(\frac{\partial w}{\partial x} - \psi \right) \frac{\partial \delta w}{\partial x} - \delta \psi \left(-m \frac{\partial w}{\partial t} \frac{\partial \delta w}{\partial t} - \rho I \frac{\partial \psi}{\partial t} \frac{\partial \delta \psi}{\partial t} \right) \right] dx dt = 0. \quad \text{Eq (70)}$$

Now the virtual displacements δw and $\delta \psi$ must both vanish at times t_0 and t_1 . Integration by parts gives

$$\begin{aligned} & \int_{t_0}^{t_1} \int_0^L \left[\frac{\partial}{\partial x} \left(EI \frac{\partial \psi}{\partial x} - kGA \left(\frac{\partial w}{\partial x} - \psi \right) + \frac{\partial}{\partial t} \rho I \frac{\partial \psi}{\partial t} \right) \delta \psi \right] dx dt \\ & + \int_{t_0}^{t_1} \int_0^L \left[\frac{\partial}{\partial x} \left(kGA \left(\frac{\partial w}{\partial x} - \psi \right) + \frac{\partial}{\partial t} m \frac{\partial w}{\partial t} \right) \delta w \right] dx dt + \int_{t_0}^t \left[EI \frac{\partial \psi}{\partial x} - \rho I \frac{\partial \psi}{\partial t} \right] \delta \psi \Big|_0^L dt \\ & + \int_{t_0}^t \left[kGA \left(\frac{\partial w}{\partial x} - \psi \right) - m \frac{\partial w}{\partial t} \right] \delta w \Big|_0^L dt = 0. \end{aligned} \quad \text{Eq (71)}$$

There will be two Euler equations of motion because there are two virtual displacements. That is

$$\frac{\partial}{\partial x} \left(EI \frac{\partial \psi}{\partial x} + kGA \left(\frac{\partial w}{\partial x} - \psi \right) - \rho I \frac{\partial^2 \psi}{\partial t^2} \right) = 0 \quad \text{Eq (72)}$$

$$m \frac{\partial^2 w}{\partial t^2} - \frac{\partial}{\partial x} kGA \frac{\partial w}{\partial x} - \psi = 0. \quad Eq (73)$$

The boundary conditions associated with the Euler equations for the free-free beam are

$$EI \frac{\partial \psi}{\partial x} = 0 \text{ and } kGA \frac{\partial w}{\partial x} - \psi = 0 \quad Eqs (74, 75)$$

since the shear and moment must be equal to zero. It is necessary to decouple the Euler equations of motion so that the variables associated with the transverse displacement and the section rotation are separated. Next, separation of variables is used to obtain the equations of time and space. Following methods laid out by Han [9], it is assumed that the time solution for the transverse displacement and the section rotation are the same

$$\begin{matrix} w(x, t) \\ \psi(x, t) \end{matrix} = T(t) \begin{matrix} W(x) \\ \psi(x) \end{matrix}. \quad Eq (76)$$

Substituting into the Euler equations and again separating variables yields the temporal and spatial solutions. The temporal solution will remain the same as in Eqs 34, 48 and the spatial solution is given as

$$\begin{matrix} 0 \\ 0 \end{matrix} = \begin{matrix} kGA & 0 \\ 0 & EI \end{matrix} \begin{matrix} W''(x) \\ \psi''(x) \end{matrix} + \begin{matrix} 0 & -kGA \\ kGA & 0 \end{matrix} \begin{matrix} W'(x) \\ \psi'(x) \end{matrix} + \begin{matrix} m\omega^2 & 0 \\ 0 & \rho I \omega^2 - kGA \end{matrix} \begin{matrix} W(x) \\ \psi(x) \end{matrix}. \quad Eq (77)$$

It is necessary to decouple once again and assume the spatial solutions for the transverse displacement and section rotation take the form

$$\begin{matrix} W(x) \\ \psi(x) \end{matrix} = d u e^{rx} \quad \begin{matrix} W'(x) \\ \psi'(x) \end{matrix} = r d u e^{rx} \quad \begin{matrix} W''(x) \\ \psi''(x) \end{matrix} = r^2 d u e^{rx} \quad Eq (78)$$

where d is a constant, u is a vector of constants, and r is a wave number. Substituting these relations into the spatial solution given in Eq 77 gives

$$\begin{matrix} kGA r^2 + m\omega^2 & -kGA r \\ kGA r & EI r^2 + \rho I \omega^2 - kGA \end{matrix} u = \begin{matrix} 0 \\ 0 \end{matrix}. \quad Eq (79)$$

To determine the non-trivial solutions to this set of equations, the determinant of the matrix in Eq 79 must be zero, which leads to the characteristic equation

$$r^4 + \frac{\rho}{E} + \frac{\rho}{kG} \omega^2 r^2 + \frac{\rho^2 \omega^4}{kGE} - \frac{m\omega^2}{EI} = 0 \quad Eq (80)$$

that has roots

$$r_i = \pm \sqrt{-\frac{1}{E} + \frac{1}{kG} \frac{\rho\omega^2}{2} \pm \sqrt{\frac{1}{E} - \frac{1}{kG} \frac{\rho^2\omega^2}{4} + \frac{m\omega^2}{EI}}}. \quad Eq (81)$$

The roots

$$r_{1,2} = \pm \sqrt{-\frac{1}{E} + \frac{1}{kG} \frac{\rho\omega^2}{2} - \sqrt{\frac{1}{E} - \frac{1}{kG} \frac{\rho^2\omega^2}{4} + \frac{m\omega^2}{EI}}}. \quad Eq (82)$$

are always imaginary, while the roots

$$r_{3,4} = \pm \sqrt{-\frac{1}{E} + \frac{1}{kG} \frac{\rho\omega^2}{2} + \sqrt{\frac{1}{E} - \frac{1}{kG} \frac{\rho^2\omega^2}{4} + \frac{m\omega^2}{EI}}}. \quad Eq (83)$$

can be real or imaginary depending upon the frequency ω . If the frequency is less than $\sqrt{\frac{kGA}{\rho I}}$ the

roots are real, but if they are greater than $\sqrt{\frac{kGA}{\rho I}}$ the roots are imaginary. This frequency is known

as the cutoff or critical frequency and is represented by the variable ω_c . The presence of this

critical frequency complicates behavior when solving for the spatial solutions. As a result, it is

necessary to break up the spatial solutions into two cases: one when $\omega > \omega_c$ and one when $\omega < \omega_c$. For $\omega < \omega_c$ with sinusoidal and hyperbolic terms instead of the exponential terms as in Eq 78 , that is

$$\begin{matrix} W(x) \\ \psi(x) \end{matrix} = \begin{matrix} C_1 \\ D_1 \end{matrix} \sin ax + \begin{matrix} C_2 \\ D_2 \end{matrix} \cos ax + \begin{matrix} C_3 \\ D_3 \end{matrix} \sinh bx + \begin{matrix} C_4 \\ D_4 \end{matrix} \cosh bx \quad \text{Eq (84)}$$

where

$$a = \sqrt{\frac{1}{E} + \frac{1}{kG} \frac{\rho\omega^2}{2} + \frac{1}{E} - \frac{1}{kG} \frac{\rho^2\omega^2}{4} + \frac{m\omega^2}{EI}} \quad \text{Eq (85)}$$

$$b = \sqrt{-\frac{1}{E} + \frac{1}{kG} \frac{\rho\omega^2}{2} + \frac{1}{E} - \frac{1}{kG} \frac{\rho^2\omega^2}{4} + \frac{m\omega^2}{EI}}. \quad \text{Eq (86)}$$

The eigenvectors of Eq 84 lead to the relations between C_i and D_i as follows

$$D_1 = -\frac{kGAa^2 - m\omega^2}{kGAa} C_2 \quad D_2 = \frac{kGAa^2 - m\omega^2}{kGAa} C_1 \quad \text{Eqs (87, 88)}$$

$$D_3 = \frac{kGAb^2 + m\omega^2}{kGAb} C_4 \quad D_4 = -\frac{kGAb^2 + m\omega^2}{kGAb} C_3. \quad \text{Eqs (89, 90)}$$

For $\omega > \omega_c$, the spatial solution only uses sinusoidal terms

$$\begin{matrix} W(x) \\ \psi(x) \end{matrix} = \begin{matrix} C_1 \\ D_1 \end{matrix} \sin ax + \begin{matrix} C_2 \\ D_2 \end{matrix} \cos ax + \begin{matrix} C_3 \\ D_3 \end{matrix} \sin bx + \begin{matrix} C_4 \\ D_4 \end{matrix} \cos bx \quad \text{Eq 91}$$

where

$$b = \sqrt{\frac{1}{E} + \frac{1}{kG} \frac{\rho\omega^2}{2} - \frac{1}{E} - \frac{1}{kG} \frac{\rho^2\omega^2}{4} + \frac{m\omega^2}{EI}} \quad \text{Eq (92)}$$

and

$$D_1 = -\frac{kGAa^2 - m\omega^2}{kGAa} C_2 \quad D_2 = \frac{kGAa^2 - m\omega^2}{kGAa} C_1 \quad \text{Eqs (93,94)}$$

$$D_3 = -\frac{kGAb^2 - m\omega^2}{kGAb} C_4 \quad D_4 = -\frac{kGAb^2 - m\omega^2}{kGAb} C_3. \quad \text{Eqs (95,96)}$$

Following the same procedure as for the Rayleigh model to obtain the equation for the natural frequency of vibration, we let

$$B_1 = \frac{\rho I \omega^2}{2E} \quad B_2 = \frac{\rho \omega^2}{2kG} \quad B_3 = \frac{m\omega^2}{EI} \quad \text{Eqs (97 - 99)}$$

so that the dispersion relationships of Eq 85 and Eq 86 become

$$a = \sqrt{B_1 + B_2 + \frac{B_1 - B_2}{2} + B_3} \quad \text{Eq (100)}$$

$$b = \sqrt{-B_1 + B_2 + \frac{B_1 - B_2}{2} + B_3}. \quad \text{Eq (101)}$$

Now, solving for B_1 , B_2 , and B_3 gives

$$B_1 = \frac{a^2 - b^2}{2(1 + \gamma^2)} \quad B_2 = \frac{\gamma^2(a^2 - b^2)}{2(1 + \gamma^2)} \quad \text{Eqs 102,103}$$

$$B_3 = \frac{1}{4} (a^2 - b^2)^2 - \frac{1 - \gamma^2}{1 + \gamma^2} (a^2 - b^2)^2 \quad \text{Eq (104)}$$

where

$$\gamma = \frac{E}{kG}. \quad \text{Eq (105)}$$

Equating the ratio of B_3 to B_1 using both *Eqs 97 – 99* and *Eqs 102 – 104* gives a relationship between the wave numbers and the slenderness ratio as follows

$$s^2 = \frac{\gamma^2 b^2 + a^2}{a^2 - b^2} \frac{\gamma^2 a^2 + b^2}{1 + \gamma^2}. \quad \text{Eq (106)}$$

Relating *Eqs 97 – 99* and *Eqs 102 – 104* also gives a new expression for *Eqs 87 – 90* as

$$D_1 = -\frac{a^2 + \gamma^2 b^2}{1 + \gamma^2} \frac{C_2}{a} \quad D_2 = \frac{a^2 + \gamma^2 b^2}{1 + \gamma^2} \frac{C_1}{a} \quad \text{Eqs (107, 108)}$$

$$D_3 = \frac{b^2 + \gamma^2 a^2}{1 + \gamma^2} \frac{C_4}{b} \quad D_4 = \frac{b^2 + \gamma^2 a^2}{1 + \gamma^2} \frac{C_3}{b}. \quad \text{Eqs (109, 110)}$$

Since it is not of concern to consider the imaginary solutions, only the case when $\omega < \omega_c$ will be examined. For a free-free beam with $\omega < \omega_c$ the frequency equation is given as

$$\frac{a^2 - b^2}{2ab} \frac{a^2 + b^2 + \gamma^2 ab - ab}{b^2 + \gamma^2 a^2} \frac{a^2 + b^2 - \gamma^2 ab + ab}{a^2 + \gamma^2 b^2} \sin a \sinh b - \cos a \cosh b + 1 = 0 \quad \text{Eq (111)}$$

Using *Eqs 97 – 99* and *Eqs 102 – 104* leads to the equation for the natural frequency for the free-free beam given as

$$\omega = \frac{1}{L} \frac{\sqrt{a^2 - b^2}}{1 + \gamma^2} \sqrt{\frac{E}{\rho}} \quad \text{Eq (112)}$$

Section 3.3: Three-Dimensional Elasticity Solutions

The solution to the three-dimensional elasticity solutions utilizes Ritz-based approximations and Hamilton's principle. Demarest, Visscher, and Heyliger proceed through derivations to give an equation for the natural frequencies [21, 22, 23]. Initially, the kinetic energy density KE and the potential energy density PE are given as

$$KE = \frac{1}{2} \rho u_j u_j \quad Eq (113)$$

$$PE = \frac{1}{2} C_{ijkl} u_{i,j} u_{k,l} \quad Eq (114)$$

where

$$u = \frac{\partial u}{\partial t}. \quad Eq (115)$$

Substituting the strain displacement relation of Eq 2 , the Cauchy stress of Eq 1 , and the definitions of the kinetic and potential energy densities into Hamilton's principle gives

$$0 = - \int_0^t \int_V \sigma_{11} \delta \epsilon_{11} + \sigma_{22} \delta \epsilon_{22} + \sigma_{33} \delta \epsilon_{33} + 2\sigma_{23} \delta \epsilon_{23} + 2\sigma_{13} \delta \epsilon_{13} + 2\sigma_{12} \delta \epsilon_{12} dV dt + \frac{1}{2} \delta \int_0^t \int_V \rho (u_1^2 + u_2^2 + u_3^2) dV dt. \quad Eq (116)$$

Ritz approximations for the displacements are expressed in the form

$$u(x, y, z, t) = \sum_{j=1}^n c_j(t) \phi_j^u(x, y, z) \quad Eq (117)$$

$$v(x, y, z, t) = \sum_{j=1}^n d_j(t) \phi_j^v(x, y, z) \quad Eq (118)$$

$$w_{x,y,z,t} = \sum_{j=1}^n e_j t \phi_j^w(x,y,z) \quad Eq (119)$$

where c , d , and e are unknown constants. The ϕ_j functions are known functions of position.

The virtual displacements take the form

$$\phi_i = x^j y^k z^l \quad Eq (120)$$

It is noteworthy to point out that the functions of time are assumed to be harmonic in order to introduce the frequency term. Substituting the displacement relations into Hamilton's principle as given in Eq 116 yields the eigenvalue problem

$$\begin{matrix} K_{11} & K_{12} & K_{13} & c & M_{11} & 0 & 0 & c \\ K_{21} & K_{22} & K_{23} & d & 0 & M_{22} & 0 & d \\ K_{31} & K_{32} & K_{33} & e & 0 & 0 & M_{33} & e \end{matrix} = \omega^2 \quad Eq (121)$$

with

$$K_{ij}^{11} = \int_V C_{11} \frac{\partial \phi_i^u}{\partial x} \frac{\partial \phi_j^u}{\partial x} + C_{55} \frac{\partial \phi_i^u}{\partial z} \frac{\partial \phi_j^u}{\partial z} + C_{66} \frac{\partial \phi_i^u}{\partial y} \frac{\partial \phi_j^u}{\partial y} dV \quad Eq (122)$$

$$K_{ij}^{12} = \int_V C_{12} \frac{\partial \phi_i^u}{\partial x} \frac{\partial \phi_j^v}{\partial y} + C_{66} \frac{\partial \phi_i^u}{\partial y} \frac{\partial \phi_j^v}{\partial x} dV \quad Eq (123)$$

$$K_{ij}^{12} = K_{ji}^{21} \quad Eq (124)$$

$$K_{ij}^{13} = \int_V C_{13} \frac{\partial \phi_i^u}{\partial x} \frac{\partial \phi_j^w}{\partial z} + C_{55} \frac{\partial \phi_i^u}{\partial z} \frac{\partial \phi_j^w}{\partial x} dV \quad Eq (125)$$

$$K_{ij}^{22} = \int_V C_{22} \frac{\partial \phi_i^v}{\partial y} \frac{\partial \phi_j^v}{\partial y} + C_{44} \frac{\partial \phi_i^v}{\partial z} \frac{\partial \phi_j^v}{\partial z} + C_{66} \frac{\partial \phi_i^v}{\partial x} \frac{\partial \phi_j^v}{\partial x} dV \quad Eq (126)$$

$$K_{ij}^{23} = \int_V C_{23} \frac{\partial \phi_i^v}{\partial y} \frac{\partial \phi_j^w}{\partial z} + C_{44} \frac{\partial \phi_i^v}{\partial z} \frac{\partial \phi_j^w}{\partial y} dV \quad Eq (127)$$

$$K_{ij}^{23} = K_{ji}^{32} \quad \text{Eq (128)}$$

$$K_{ij}^{33} = \int_V C_{33} \frac{\partial \phi_i^w}{\partial z} \frac{\partial \phi_j^w}{\partial z} + C_{44} \frac{\partial \phi_i^w}{\partial y} \frac{\partial \phi_j^w}{\partial y} + C_{55} \frac{\partial \phi_i^w}{\partial x} \frac{\partial \phi_j^w}{\partial x} dV \quad \text{Eq (129)}$$

$$M_{ij}^{11} = M_{ij}^{22} = M_{ij}^{33} = \int_V \phi_i \phi_j dV. \quad \text{Eq (130)}$$

Solving this system of equations for ω yields the natural frequencies.

Section 3.4: Computations

FORTRAN coding was utilized to obtain the natural frequencies for a number of beam geometries. All properties of the material composition and beam geometry were inputted into the code. Using the derived equations, the natural frequencies could be calculated. Initially, the individual codes for the Euler-Bernoulli, Rayleigh, Timoshenko, and elasticity solutions were tested for solid isotropic and anisotropic sections to ensure no fundamental flaws were present. To ensure accuracy, the frequencies were cross-referenced with those calculated in Heyliger's unpublished study. At this point, each of the codes were altered to account for the hollow sections.

The Euler-Bernoulli code was the most simple, needing only 34 lines of code in order to produce the first five natural frequencies. The code for the Rayleigh beam needed 462 lines of code, while the Timoshenko theory needed just 57 lines. The elasticity solutions contained 664 lines of code and a separate input file that varied in size depending on the beam length. The code for

the elasticity solutions contains the calculations of the eigenvalue problem given in Eq (121) for a 6 X 6 stiffness matrix. Using the Rayleigh and Timoshenko codes, only one frequency could be obtained at a time, further increasing the computational demand. The code for the elasticity solutions calculates hundreds of frequencies with each run. When altering the codes to adjust for changes in geometry, the codes vary in terms of the maintenance necessary to make the adjustments. For the Euler-Bernoulli and Rayleigh codes, only the wall thicknesses and lengths have to be changed. The Timoshenko code has to include the shape factor as well. The elasticity code is the most demanding and time consuming when switching beam sizes.

For plotting of mode shapes and cross-section deformations, the elasticity code is used. An input file has to be changed in order to accommodate each beam size. A number of lines of code have to be adjusted depending on which mode shape is to be plotted, not just the beam dimensions as was the case for the frequency analysis.

Chapter 4

Results and Discussion

To compare the three beam theories with the elasticity solutions, four beam cross-sections and seven beam lengths were used. It is important to consider shorter beams as well as long, slender beams to examine when it is appropriate to use each respective theory. The hollow cross-sections had wall thicknesses that varied in width from 0.0005 m to 0.004 m. The outside dimensions of each beam were 0.01 m X 0.01 m. Beam lengths varied from 0.01 m to 1.0 m. A wide variety of hollow beam sizes were necessary for computational analysis to determine when it is appropriate to use the specific beam theories. Table 2. shows the four undeformed beam cross-sections and the respective radius of gyration for each case. Graphite-magnesium was the anisotropic material used to model the beams. Graphite-magnesium has a mass density of 1738 kg/m³ and components of the elastic stiffness tensor as follows

$$C_{11} = C_{22} = 28.19 \text{ GPa}, C_{33} = 174.3 \text{ GPa}, C_{44} = C_{55} = 17.91 \text{ GPa}$$

$$C_{66} = 8.76 \text{ GPa}, C_{12} = 10.67 \text{ GPa}, C_{13} = C_{23} = 12.2 \text{ GPa}.$$

Steel was used to model the isotropic beams for comparative purposes. Steel has a density of 7830 kg/m³ and components of the elastic stiffness tensor as follows

$$C_{11} = 269.23 \text{ GPa}, C_{44} = 76.92 \text{ GPa}.$$

A Poisson's ratio of zero was used in the analysis of the approximate beam theories. Neglecting the Poisson effect, which accounts for the three dimensional deformation of a solid, allows for a straightforward comparison between the three approximate beam theories. The components of the elastic stiffness tensor listed previously include the Poisson effect.

As discussed in detail previously, the Timoshenko model utilizes the shear or shape factor. For the purposes of this testing, a shear factor of 0.8442 was used for the anisotropic beams as calculated from the equation given by Pucheggar [15]. An evaluation of the appropriateness of using this shape factor will be presented in the conclusions.

For each wall thickness and cross-section, the first five non-zero natural frequencies were calculated using the derived frequency equations as given in *Eq 39* , *Eq 62* , *Eq 112* , and *Eq 121* . These anisotropic frequencies are tabulated in Tables 3 through 6 and the isotropic frequencies are tabulated in Tables 7 through 10. In these tables, EB stands for the Euler-Bernoulli model and Full represents the full three-dimensional elasticity solutions. For the anisotropic beam with length of 1.0 m and wall thickness of 0.0005 m, the natural frequencies could not be calculated for the elasticity solutions because the matrix was not positive-definite. This is likely attributable to the thin walls and thin cross-sectional area of this beam.

It is clear from Tables 3 through 10 that the natural frequencies are reduced as beams increase in length and cross sectional area. When the beam length is kept constant and the cross-sectional area is varied, a noticeable behavior occurs. The percent error for each beam theory in calculating the natural frequencies as compared to full elasticity solutions is typically reduced as the cross-sectional area increases. Not only is the accuracy of the approximate methods dependent on the length of the beam as others have suggested, but on the wall-thickness, and

correspondingly, the cross-sectional area as well. In looking at the definition of the slenderness ratio as given in Eq 60 , one can see that the length is directly related to the slenderness ratio, while only the root of the area is related. Nevertheless, both factors contribute significantly to the slenderness ratio. The percent error as a function of the inverse of the slenderness ratio is plotted for the first mode of vibration in Figures 1 through 4 to demonstrate this behavior.

It is clear for each beam that the Timoshenko model gives the best approximation to elasticity solutions. The inclusion of the shear coefficient proves pivotal in accurately calculating the frequencies, especially for short and stocky beams. More will be discussed on this issue later. The plots of the percent error also show that the Rayleigh beam model, which adds the rotary inertia term, does not provide a significant improvement over the more simple Euler-Bernoulli beam method.

In most instances, Tables 3 through 10 give natural frequencies that are greater than those provided by elasticity methods. This behavior, where the computed natural frequencies approach the true values from above, is to be expected. Frequency can be defined as

$$\omega = \frac{k}{m} \quad \text{Eq (131)}$$

with k defined as the stiffness and m defined as the mass. Each beam theory limits the deflection of the beam, or in essence, makes the beam stiffer. From this equation, it is clear that as the stiffness increases, the frequencies will become larger. Since the Euler-Bernoulli model limits the flexibility of the beam the most, one would expect it to produce the highest natural frequencies. Tables 3 through 10 and a plot of the scaled natural frequencies as given in Figures 5 through 8 depict that this is indeed the case. The Rayleigh model relaxes the constraints on the

movement of the beam with the inclusion of the rotary inertia and effectively reduces the stiffness. As a result, one would expect natural frequencies to be less than those predicted by the Euler-Bernoulli model. Again Tables 3 through 10 and Figures 5 through 8 demonstrate that this is indeed the case. The Timoshenko model further reduces the stiffness of the beam with the inclusion of the shear term. Again this reduces the natural frequencies.

Some unexpected behavior occurs with the results of the natural frequencies for the Timoshenko model for the isotropic beam. While the natural frequencies are lower than those calculated by the Euler-Bernoulli and Rayleigh models, Tables 7 through 10 show that the natural frequencies for a number of beam lengths are lower than elasticity solutions. This probably results from an underestimation of the strain energy term. The strain energy contains the stiffness term that is located in the numerator of $Eq\ 131$. With the strain energy, and thus the stiffness too small, it is possible that the Timoshenko beam theory can produce natural frequencies that are below those of elasticity solutions. Table 11 shows the percent error of the natural frequencies for the three beam theories as compared to the full elasticity solutions for the anisotropic beam. The percent error for the isotropic beam is given in Table 12. For the cells with green shading, the error is within five percent of elasticity solutions, blue cells have error between five and fifty percent, and cells shaded red have error greater than fifty percent. As evident from these two tables, less error is associated with beams of larger wall thicknesses, longer lengths, and lower modes.

As expected, the percent error for the three beam models decreases as the slenderness ratio increases. The longer and more slender a beam becomes, the less significant is the deflection resulting from shear effects. This fact becomes clear in looking at a plot of the scaled natural frequencies as shown in Figures 5 through 8. For large slenderness ratios, where the inverse of

the slenderness ratio is small, the three beam theories produce results very similar to those produced by elasticity solutions. As the beams shrink in length, the approximate theories stray noticeably.

In examining the frequency analysis for higher order modes of vibration, it becomes evident that the reliability on the approximate methods to produce accurate results is inextricably linked to the slenderness ratio. Not only is more error introduced with stocky beams, but that error generally increases with increasing mode numbers, though there were exceptions. For the beams with a length of 1.0 m, each of the approximate beam theories provided adequate results, having percent error in calculating the natural frequency for the fifth mode of vibration of less than four percent.* However, for the shortest beams, the Euler-Bernoulli model produced errors of nearly 2,300 percent for the fifth mode of vibration. The Rayleigh method produced errors of nearly 450 percent for the fifth mode of vibration and the Timoshenko model produced errors of nearly 44 percent for the fifth mode of vibration on the shortest beam. Plotting results for the higher modes of vibration would not show any significantly different behavior from that of the first mode. The only differences from Figures 1 through 4 would be that the approximate methods would show even more error for higher modes at the same slenderness ratios. Replicating Figures 5 through 8 for higher modes would look nearly the same, except that the approximate methods would begin to stray from the elasticity solutions sooner.

The first five flexural mode shapes were plotted for the case with beam length of 0.20 m and wall thickness of 0.002 m. These mode shapes depict the deformation that will occur to the beam when excited at the specific natural frequencies given in Table 5. Figures 9 through 13

* Percent error could not be calculated for beam with length 1.0 m and wall thickness of 0.0005 m because of positive definite matrix

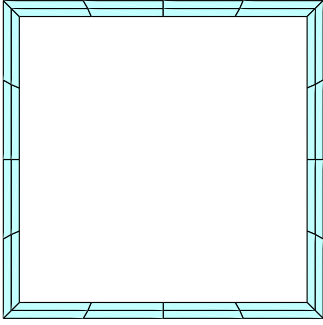
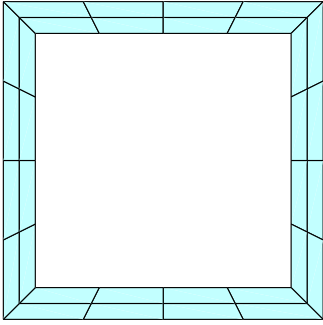
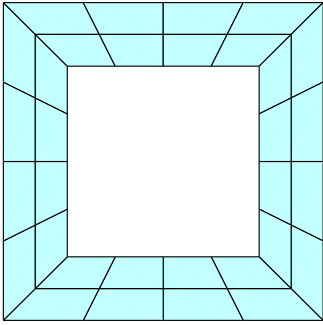
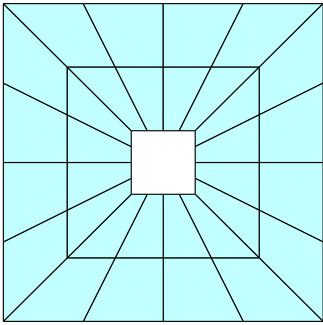
contain the plots of the mode shapes. The first five flexural mode shapes were also plotted for a beam with length of 0.05 m and wall thickness of 0.001 m. These plots can be seen in Figures 14 through 18. Modes one, three, and five are called the symmetric modes, because their shape is symmetric about the midpoint of the beam. Modes two and four are called the antisymmetric modes because their deflected shape is not symmetric about the midpoint of the beam.

The first mode of vibration is regarded as the most important mode because it will dominate the motion. For taller, more slender structures, the higher order modes can be excited. Tall buildings can provide such behavior under earthquake or wind loadings. In comparing the plots of the mode shapes with beam lengths of 0.20 m and 0.05 m, greater amplitudes of deformation are noticeable for the longer beam. For the longer beam, less deformation occurs to the cross-section because it is more difficult to bend the beam about the strong axis. With the short beam, lower amplitudes of deformation occur to the beam length while more deformation occurs to the cross-section.

Plots of the undeformed beam cross-sections can be seen in Table 12. The deformed cross-sections are plotted for three beam lengths and four wall thicknesses for each of the first five modes of vibration in Tables 13 through 17. These plots show that less distortion to the hollow beam cross-section occurs for lower order modes of vibration. Also, as the beam length and cross-sectional areas increase, less deformation is present. This is attributable once again to the increased slenderness ratio. It is safe to assume that if similar plots were made for shorter beams, more deformation would occur, and for longer, more slender beams, less deformation would occur. Tables 13 through 17 also show that there is no distinct pattern as to how the cross-section will deform. In some cases the top of the beam collapses inward, while in others the bottom of the beam folds upward. This poses a problem similar in nature to a long beam

vibrating back and forth. As the input frequency is increased, higher modes of vibration will be excited and the cross-sectional distortion will force the beam walls to fold in and out. This back and forth motion could potentially cause localized buckling of the beam's walls. As with the design of structures, these higher order modes are less likely to be excited, but nevertheless, they are important enough that they cannot be disregarded.

Table 2. Undeformed Cross-sections

Wall Thickness (m)		Radius of Gyration (m)
0.0005		0.00388
0.001		0.00370
0.002		0.00337
0.004		0.00294

Note: The outside dimensions of each cross-section are 0.01 m X 0.01 m

Table 3. Dimensionless Natural Frequencies--Wall Thickness 0.0005 m (Anisotropic)

	Flexural Mode	EB	Rayleigh	Timoshenko	Full
L=.01	1	8,508,198.4	2,896,831.3	1,121,794.1	925,730.7
	2	23,453,544.5	5,783,522.9	1,731,578.1	1,125,322.3
	3	45,978,042.4	8,945,498.4	2,665,146.0	1,794,892.7
	4	76,004,113.6	12,068,058.2	3,021,510.3	2,688,227.7
	5	113,537,470.0	15,188,245.2	3,578,000.3	4,750,597.3
L=.02	1	2,127,049.6	1,250,043.5	802,574.5	409,230.0
	2	5,863,386.1	2,607,496.4	821,513.4	543,853.8
	3	11,494,510.6	4,161,758.5	1,346,080.9	668,646.4
	4	19,001,028.4	5,747,235.8	1,582,533.3	1,021,037.3
	5	28,384,367.5	7,338,791.1	1,851,363.0	1,335,596.7
L=.05	1	340,327.9	298,474.6	240,503.7	261,822.4
	2	938,141.7	727,727.2	436,467.3	362,519.6
	3	1,839,121.6	1,262,660.9	645,632.4	397,399.2
	4	3,040,164.3	1,854,964.6	738,850.0	480,122.3
	5	4,541,498.5	2,479,844.7	902,545.4	546,279.5
L=.10	1	85,082.0	82,070.8	75,560.9	65,150.2
	2	234,535.4	217,307.3	170,654.5	103,632.6
	3	459,780.4	406,012.4	274,564.6	280,673.7
	4	760,041.1	635,741.2	377,006.4	353,103.6
	5	1,135,374.6	896,319.2	477,570.2	357,785.3
L=.20	1	21,270.5	21,075.0	20,573.3	20,034.7
	2	58,633.9	57,464.3	52,909.1	48,005.4
	3	114,945.1	111,094.5	94,920.1	76,285.6
	4	190,010.3	180,559.1	142,158.4	100,703.4
	5	283,843.7	264,484.3	191,947.4	115,148.1
L=.40	1	5,317.6	5,305.3	5,272.0	5,241.0
	2	14,658.5	14,583.7	14,252.4	13,944.5
	3	28,736.3	28,486.5	27,163.8	25,915.4
	4	47,502.6	46,877.6	43,329.1	40,142.4
	5	70,960.9	69,652.2	62,102.7	55,327.8
L=1.0	1	850.8	850.5	849.6	
	2	2,345.4	2,343.4	2,334.5	
	3	4,597.8	4,591.4	4,554.2	
	4	7,600.4	7,584.2	7,479.0	
	5	11,353.7	11,319.4	11,081.5	

Note: The first five flexural frequencies are listed for the anisotropic graphite-magnesium.
All units of length are given in meters

Table 4. Dimensionless Natural Frequencies--Wall Thickness 0.001 m (Anisotropic)

	Flexural Mode	EB	Rayleigh	Timoshenko	Full
L=.01	1	8,098,792.3	2,879,927.7	1,142,992.9	1,098,817.9
	2	22,324,983.1	5,755,442.5	1,727,638.0	1,572,846.9
	3	43,765,624.4	8,919,116.9	2,665,638.7	2,829,909.4
	4	72,346,870.7	12,045,363.7	3,028,453.0	3,647,158.5
	5	108,074,159.0	15,169,022.4	3,581,385.9	4,730,907.6
L=.02	1	2,024,698.1	1,228,473.5	816,932.9	715,709.4
	2	5,581,245.8	2,578,522.3	828,348.1	964,494.7
	3	10,941,406.1	4,127,010.9	1,349,199.9	1,282,486.4
	4	18,086,717.7	5,712,795.3	1,588,667.0	1,350,633.5
	5	27,018,539.8	7,306,669.6	1,861,790.4	1,810,717.4
L=.05	1	323,951.7	287,255.9	234,179.6	182,740.9
	2	892,999.3	706,061.0	432,877.1	431,896.5
	3	1,750,624.9	1,232,488.8	641,678.0	619,737.5
	4	2,893,874.6	1,818,850.0	758,249.1	776,778.6
	5	4,322,966.0	2,439,960.2	912,855.1	899,088.6
L=.10	1	80,987.9	78,378.4	72,626.8	67,943.8
	2	223,249.8	208,242.5	166,087.7	138,557.9
	3	437,656.2	390,536.0	269,439.7	198,793.6
	4	723,468.7	613,842.0	372,204.7	253,077.4
	5	1,080,741.5	868,581.1	473,289.9	295,652.8
L=.20	1	20,247.0	20,078.2	19,642.3	19,293.1
	2	55,812.5	54,801.0	50,802.0	47,924.2
	3	109,414.1	106,077.7	91,704.5	82,371.5
	4	180,867.2	172,659.4	138,138.4	118,779.4
	5	270,185.4	253,329.7	187,440.3	153,632.2
L=.40	1	5,061.7	5,051.1	5,022.4	4,999.3
	2	13,953.1	13,888.6	13,601.3	13,381.1
	3	27,353.5	27,137.8	25,985.9	25,139.5
	4	45,216.8	44,676.8	41,569.5	39,470.5
	5	67,546.3	66,414.7	59,764.8	55,541.2
L=1.0	1	809.9	809.6	808.9	808.3
	2	2,232.5	2,230.8	2,223.2	2,217.1
	3	4,376.6	4,371.0	4,338.9	4,314.0
	4	7,234.7	7,220.7	7,129.8	7,061.9
	5	10,807.4	10,777.8	10,571.7	10,420.6

Note: The first five flexural frequencies are listed for the anisotropic graphite-magnesium.
All units of length are given in meters

Table 5. Dimensionless Natural Frequencies--Wall Thickness 0.002 m (Anisotropic)

	Flexural Mode	EB	Rayleigh	Timoshenko	Full
L=.01	1	7,375,097.8	2,843,857.7	1,187,910.0	1,294,272.8
	2	20,330,060.0	5,697,664.2	1,719,284.0	2,181,280.1
	3	39,854,801.6	8,862,909.5	2,666,813.4	3,287,391.3
	4	65,882,075.6	11,996,549.0	3,043,098.6	4,225,871.6
	5	98,416,833.3	15,127,340.1	3,589,055.2	5,236,653.7
L=.02	1	1,843,774.4	1,184,799.9	801,987.7	617,640.5
	2	5,082,515.0	2,519,463.3	880,041.8	975,284.0
	3	9,963,700.4	4,055,513.6	1,357,375.3	1,450,010.6
	4	16,470,518.9	5,640,629.3	1,599,845.7	1,963,287.5
	5	24,604,208.3	7,238,488.5	1,885,619.1	3,335,808.9
L=.05	1	295,003.9	266,512.1	221,993.6	201,585.9
	2	813,202.3	664,631.6	424,254.6	357,299.5
	3	1,594,191.9	1,173,492.2	633,012.3	520,829.5
	4	2,635,282.8	1,747,125.1	785,810.6	725,374.1
	5	3,936,673.0	2,359,743.6	945,411.7	829,200.1
L=.10	1	73,751.0	71,764.7	67,240.0	64,867.2
	2	203,300.6	191,777.8	157,246.2	143,501.7
	3	398,548.0	361,992.9	259,172.0	227,195.7
	4	658,820.7	572,824.5	362,190.7	310,835.5
	5	984,168.3	815,870.1	464,084.2	392,262.8
L=.20	1	18,437.7	18,310.0	17,976.9	17,787.2
	2	50,825.1	50,057.9	46,946.3	45,376.1
	3	99,637.0	97,098.2	85,673.3	80,608.9
	4	164,705.2	158,435.7	130,418.1	119,958.6
	5	246,042.1	233,110.6	178,603.6	160,856.5
L=.40	1	4,609.4	4,601.4	4,579.6	4,566.9
	2	12,706.3	12,657.5	12,438.7	12,317.1
	3	24,909.2	24,746.1	23,861.8	23,392.8
	4	41,176.3	40,767.3	38,359.9	37,195.8
	5	61,510.5	60,652.3	55,447.7	53,096.9
L=1.0	1	737.5	737.3	736.7	736.4
	2	2,033.0	2,031.7	2,025.9	2,022.6
	3	3,985.5	3,981.3	3,957.0	3,943.2
	4	6,588.2	6,577.6	6,508.6	6,471.4
	5	9,841.7	9,819.3	9,662.6	9,579.6

Note: The first five flexural frequencies are listed for the anisotropic graphite-magnesium.
All units of length are given in meters

Table 6. Dimensionless Natural Frequencies--Wall Thickness 0.004 m (Anisotropic)

	Flexural Mode	EB	Rayleigh	Timoshenko	Full
L=.01	1	6,449,335.9	2,782,052.6	1,264,075.1	1,713,931.6
	2	17,778,121.7	5,603,956.9	1,705,133.8	1,176,389.9
	3	34,852,012.7	8,766,747.1	2,669,272.1	3,343,966.4
	4	57,612,203.5	11,911,512.2	3,067,581.2	2,913,778.5
	5	86,063,023.6	15,053,729.0	3,603,733.2	4,340,298.5
L=.02	1	1,612,334.0	1,116,504.3	775,225.5	760,951.1
	2	4,444,530.4	2,424,969.5	954,462.5	1,355,770.7
	3	8,713,003.2	3,939,803.4	1,377,444.1	1,665,487.9
	4	14,403,050.9	5,520,535.2	1,613,985.8	2,236,926.3
	5	21,515,755.9	7,122,566.8	1,930,628.3	2,955,171.3
L=.05	1	257,973.4	238,284.0	204,311.3	202,481.1
	2	711,124.8	605,391.8	408,437.2	402,924.8
	3	1,394,080.4	1,085,991.4	617,838.3	611,658.3
	4	2,304,488.0	1,637,880.5	799,660.4	792,615.2
	5	3,442,520.7	2,234,998.1	989,298.4	997,299.8
L=.10	1	64,493.4	63,153.0	59,976.2	59,763.2
	2	177,781.2	169,925.0	144,371.8	143,147.9
	3	348,520.1	323,285.3	243,379.0	240,567.3
	4	576,122.0	515,935.0	345,932.9	342,260.7
	5	860,630.2	741,150.3	448,500.2	444,203.8
L=.20	1	16,123.3	16,037.8	15,811.8	15,795.2
	2	44,445.3	43,929.5	41,773.8	41,641.7
	3	87,130.0	85,417.3	77,288.3	76,849.4
	4	144,030.5	139,782.1	119,299.2	118,465.8
	5	215,157.5	206,349.5	165,465.3	164,055.6
L=.40	1	4,030.8	4,025.5	4,010.9	4,009.8
	2	11,111.3	11,078.7	10,930.9	10,921.0
	3	21,782.5	21,673.1	21,070.5	21,032.3
	4	36,007.6	35,733.2	34,074.0	33,987.2
	5	53,789.4	53,212.7	49,580.7	49,403.5
L=1.0	1	644.9	644.8	644.4	644.4
	2	1,777.8	1,777.0	1,773.1	1,772.8
	3	3,485.2	3,482.4	3,466.1	3,465.0
	4	5,761.2	5,754.1	5,707.8	5,705.1
	5	8,606.3	8,591.3	8,485.7	8,479.8

Note: The first five flexural frequencies are listed for the anisotropic graphite-magnesium.
All units of length are given in meters

Table 7. Dimensionless Natural Frequencies--Wall Thickness 0.0005 m (Isotropic)

	Flexural Mode	EB	Rayleigh	Timoshenko	Full
L=.01	1	4,391,440.3	1,495,176.9	757,567.0	637,298.7
	2	12,105,364.4	2,985,120.3	1,108,075.7	916,622.8
	3	23,731,208.6	4,617,149.3	1,600,774.1	1,280,534.1
	4	39,228,931.4	6,228,834.3	1,766,730.2	1,496,147.3
	5	58,601,481.0	7,839,294.5	2,367,920.9	2,097,193.2
L=.02	1	1,097,860.1	645,200.2	510,304.7	485,067.8
	2	3,026,341.1	1,345,839.0	545,390.9	574,741.5
	3	5,932,802.1	2,148,059.3	888,333.9	678,735.6
	4	9,807,232.9	2,966,391.0	910,759.2	895,065.3
	5	14,650,370.2	3,787,859.9	1,202,357.0	920,886.8
L=.05	1	175,657.6	154,055.4	135,414.2	113,896.3
	2	484,214.5	375,610.7	269,452.1	155,604.4
	3	949,248.3	651,712.6	408,283.1	177,652.1
	4	1,569,157.1	957,425.5	496,819.6	222,099.1
	5	2,344,059.1	1,279,952.5	596,543.4	256,530.7
L=.10	1	43,914.4	42,360.2	40,368.3	39,903.9
	2	121,053.6	112,161.4	96,712.4	90,128.4
	3	237,312.1	209,560.1	162,951.2	128,655.6
	4	392,289.3	328,132.9	231,764.5	157,811.3
	5	586,014.8	462,628.2	300,668.1	167,683.1
L=.20	1	10,978.6	10,877.7	10,728.9	10,725.0
	2	30,263.4	29,659.8	28,262.2	28,158.2
	3	59,328.0	57,340.6	52,168.1	51,327.7
	4	98,072.3	93,194.1	80,403.7	77,696.5
	5	146,503.7	136,511.5	111,441.8	103,491.5
L=.40	1	2,744.7	2,738.3	2,728.5	2,728.8
	2	7,565.9	7,527.3	7,429.1	7,430.9
	3	14,832.0	14,703.1	14,305.0	14,302.9
	4	24,518.1	24,195.5	23,107.6	23,095.4
	5	36,625.9	35,950.4	33,587.8	33,501.0
L=1.0	1	439.1	439.0	438.7	438.7
	2	1,210.5	1,209.5	1,206.9	1,207.1
	3	2,373.1	2,369.8	2,358.9	2,359.4
	4	3,922.9	3,914.5	3,883.5	3,885.1
	5	5,860.1	5,842.4	5,772.0	5,775.4

Note: The first five flexural frequencies are listed for the isotropic steel.
All units of length are given in meters

Table 8. Dimensionless Natural Frequencies--Wall Thickness 0.001 m (Isotropic)

	Flexural Mode	EB	Rayleigh	Timoshenko	Full
L=.01	1	4,180,128.6	1,486,452.3	772,460.9	1,118,469.6
	2	11,522,866.2	2,970,626.8	1,103,058.6	1,082,172.0
	3	22,589,286.2	4,603,532.7	1,611,200.2	1,711,546.4
	4	37,341,273.9	6,217,120.7	1,766,544.2	2,515,013.7
	5	55,781,635.6	7,829,372.8	2,368,820.6	2,889,490.4
L=.02	1	1,045,032.1	634,067.0	502,929.8	363,712.5
	2	2,880,716.5	1,330,884.2	562,684.8	516,052.7
	3	5,647,321.6	2,130,124.5	890,414.3	698,071.3
	4	9,335,318.5	2,948,614.8	921,683.6	962,197.8
	5	13,945,408.9	3,771,280.6	1,205,861.3	1,251,027.3
L=.05	1	167,205.1	148,264.9	131,250.1	129,377.2
	2	460,914.6	364,427.9	265,542.0	246,870.8
	3	903,571.4	636,139.5	404,856.6	330,694.6
	4	1,493,650.9	938,785.3	506,221.4	413,958.0
	5	2,231,265.3	1,259,366.5	607,012.4	482,441.3
L=.10	1	41,801.3	40,454.4	38,700.1	38,757.3
	2	115,228.7	107,482.8	93,614.9	93,620.7
	3	225,892.8	201,572.1	158,969.3	156,592.6
	4	373,412.7	316,829.8	227,510.7	220,457.4
	5	557,816.3	448,311.4	296,535.0	276,644.9
L=.20	1	10,450.3	10,363.2	10,234.1	10,243.4
	2	28,807.2	28,285.1	27,062.8	27,143.1
	3	56,473.2	54,751.2	50,182.4	50,398.3
	4	93,353.2	89,116.8	77,704.6	78,202.2
	5	139,454.1	130,754.2	108,169.6	108,732.1
L=.40	1	2,612.6	2,607.1	2,598.7	2,599.4
	2	7,201.8	7,168.5	7,083.5	7,090.8
	3	14,118.3	14,007.0	13,661.1	13,689.3
	4	23,338.3	23,059.6	22,110.5	22,193.2
	5	34,863.5	34,279.4	32,209.0	32,378.2
L=1.0	1	418.0	417.9	417.7	417.7
	2	1,152.3	1,151.4	1,149.2	1,149.4
	3	2,258.9	2,256.1	2,246.6	2,247.5
	4	3,734.1	3,726.9	3,700.1	3,702.9
	5	5,578.2	5,562.9	5,501.9	5,508.2

Note: The first five flexural frequencies are listed for the isotropic steel.
All units of length are given in meters

Table 9. Dimensionless Natural Frequencies--Wall Thickness 0.002 m (Isotropic)

	Flexural Mode	EB	Rayleigh	Timoshenko	Full
L=.01	1	3,806,599.3	1,467,835.0	803,927.7	1,049,709.1
	2	10,493,202.2	2,940,805.0	1,092,966.4	1,740,655.3
	3	20,570,745.5	4,574,521.7	1,632,977.4	2,525,834.7
	4	34,004,520.3	6,191,925.3	1,766,260.2	3,287,580.5
	5	50,797,082.1	7,807,858.8	2,370,877.5	3,592,310.0
L=.02	1	951,649.8	611,525.2	488,209.6	493,844.2
	2	2,623,300.5	1,300,401.4	596,351.9	633,226.4
	3	5,142,686.4	2,093,221.8	896,366.6	852,602.8
	4	8,501,130.1	2,911,366.9	943,087.5	882,584.4
	5	12,699,270.5	3,736,089.5	1,214,420.8	1,189,987.2
L=.05	1	152,264.0	137,558.2	123,377.1	125,588.4
	2	419,728.1	343,044.4	257,153.8	268,238.1
	3	822,829.8	605,688.8	397,125.9	417,208.2
	4	1,360,180.7	901,765.0	515,951.9	552,657.6
	5	2,031,883.1	1,217,963.3	628,880.5	672,454.4
L=.10	1	38,066.0	37,040.8	35,668.5	35,917.6
	2	104,932.0	98,984.6	87,762.2	89,662.7
	3	205,707.4	186,839.8	151,201.6	156,538.7
	4	340,045.2	295,658.9	218,942.1	229,944.4
	5	507,970.8	421,105.0	287,935.7	305,191.9
L=.20	1	9,516.5	9,450.6	9,352.1	9,370.9
	2	26,233.0	25,837.0	24,892.1	25,072.4
	3	51,426.9	50,116.5	46,523.6	47,179.9
	4	85,011.3	81,775.3	72,639.2	74,315.9
	5	126,992.7	120,318.2	101,921.2	105,140.7
L=.40	1	2,379.1	2,375.0	2,368.6	2,369.8
	2	6,558.3	6,533.1	6,468.4	6,481.3
	3	12,856.7	12,772.5	12,508.1	12,560.1
	4	21,252.8	21,041.7	20,311.3	20,460.4
	5	31,748.2	31,305.2	29,699.1	30,023.5
L=1.0	1	380.7	380.6	380.4	380.4
	2	1,049.3	1,048.7	1,047.0	1,047.3
	3	2,057.1	2,054.9	2,047.8	2,049.2
	4	3,400.5	3,395.0	3,374.7	3,379.0
	5	5,079.7	5,068.2	5,021.9	5,031.8

Note: The first five flexural frequencies are listed for the isotropic steel.
All units of length are given in meters

Table 10. Dimensionless Natural Frequencies--Wall Thickness 0.004 m (Isotropic)

	Flexural Mode	EB	Rayleigh	Timoshenko	Full
L=.01	1	3,328,774.5	1,435,934.8	857,025.2	1,289,693.0
	2	9,176,039.1	2,892,438.7	1,077,313.7	2,198,843.1
	3	17,988,595.0	4,524,888.3	1,669,083.2	2,677,970.4
	4	29,736,090.2	6,148,034.3	1,766,183.1	2,723,232.0
	5	44,420,759.4	7,769,865.0	2,374,886.6	3,522,333.7
L=.02	1	832,193.6	576,275.0	465,526.8	515,036.6
	2	2,294,009.8	1,251,629.1	641,320.0	830,878.6
	3	4,497,148.7	2,033,498.9	912,394.3	1,197,539.2
	4	7,434,022.6	2,849,381.3	974,055.2	1,230,420.2
	5	11,105,189.9	3,676,257.4	1,232,847.5	1,311,148.5
L=.05	1	133,151.0	122,988.5	112,272.9	116,943.8
	2	367,041.5	312,468.3	243,384.8	270,903.1
	3	719,543.7	560,526.0	383,489.3	447,773.4
	4	1,189,443.5	845,379.2	514,603.4	628,086.0
	5	1,776,830.2	1,153,576.9	640,203.6	802,567.5
L=.10	1	33,287.7	32,595.9	31,639.3	32,070.8
	2	91,760.4	87,705.5	79,536.7	83,077.5
	3	179,885.9	166,861.2	139,744.7	150,856.8
	4	297,360.9	266,295.8	205,713.0	229,465.1
	5	444,207.6	382,538.9	274,078.0	314,571.0
L=.20	1	8,321.9	8,277.8	8,211.2	8,241.7
	2	22,940.1	22,673.9	22,024.4	22,319.7
	3	44,971.5	44,087.5	41,565.8	42,688.0
	4	74,340.2	72,147.4	65,588.5	68,458.9
	5	111,051.9	106,505.7	92,995.5	98,742.6
L=.40	1	2,080.5	2,077.7	2,073.4	2,075.4
	2	5,735.0	5,718.2	5,674.6	5,694.7
	3	11,242.9	11,186.4	11,007.2	11,089.5
	4	18,585.1	18,443.4	17,944.0	18,173.8
	5	27,763.0	27,465.3	26,356.8	26,862.2
L=1.0	1	332.9	332.8	332.7	332.8
	2	917.6	917.2	916.0	916.6
	3	1,798.9	1,797.4	1,792.6	1,794.9
	4	2,973.6	2,970.0	2,956.3	2,962.7
	5	4,442.1	4,434.3	4,403.2	4,417.8

Note: The first five flexural frequencies are listed for the isotropic steel.
All units of length are given in meters

Table 11. Percent Error from Elasticity Solutions (Anisotropic)

Beam Length (m)	Flexural Mode Number	Wall Thickness (m)											
		0.0005			0.001			0.002			0.004		
		EB	Ray	Timo	EB	Ray	Timo	EB	Ray	Timo	EB	Ray	Timo
L=.01	1	-819.08	-212.92	-21.18	-637.05	-162.09	-4.02	-469.83	-119.73	8.22	-276.29	-62.32	26.25
	2	-1984.16	-413.94	-53.87	-1319.40	-265.93	-9.84	-832.02	-161.21	21.18	-1411.24	-376.37	-44.95
	3	-2461.60	-398.39	-48.48	-1446.54	-215.17	5.80	-1112.35	-169.60	18.88	-942.24	-162.17	20.18
	4	-2727.29	-348.92	-12.40	-1883.65	-230.27	16.96	-1459.02	-183.88	27.99	-1877.23	-308.80	-5.28
	5	-2289.96	-219.71	24.68	-2184.43	-220.64	24.30	-1779.38	-188.87	31.46	-1882.88	-246.84	16.97
L=.02	1	-419.77	-205.46	-96.12	-182.89	-71.64	-14.14	-198.52	-91.83	-29.85	-111.88	-46.72	-1.88
	2	-978.12	-379.45	-51.05	-478.67	-167.34	14.12	-421.13	-158.33	9.77	-227.82	-78.86	29.60
	3	-1619.07	-522.42	-101.31	-753.14	-221.80	-5.20	-587.15	-179.69	6.39	-423.15	-136.56	17.29
	4	-1760.95	-462.88	-54.99	-1239.13	-322.97	-17.62	-738.93	-187.31	18.51	-543.88	-146.79	27.85
	5	-2025.22	-449.48	-38.62	-1392.15	-303.52	-2.82	-637.58	-116.99	43.47	-628.07	-141.02	34.67
L=.05	1	-29.98	-14.00	8.14	-77.27	-57.19	-28.15	-46.34	-32.21	-10.12	-27.41	-17.68	-0.90
	2	-158.78	-100.74	-20.40	-106.76	-63.48	-0.23	-127.60	-86.02	-18.74	-76.49	-50.25	-1.37
	3	-362.79	-217.73	-62.46	-182.48	-98.87	-3.54	-206.09	-125.31	-21.54	-127.92	-77.55	-1.01
	4	-533.21	-286.35	-53.89	-272.55	-134.15	2.39	-263.30	-140.86	-8.33	-190.74	-106.64	-0.89
	5	-731.35	-353.95	-65.22	-380.82	-171.38	-1.53	-374.76	-184.58	-14.01	-245.18	-124.10	0.80
L=.10	1	-30.59	-25.97	-15.98	-19.20	-15.36	-6.89	-13.70	-10.63	-3.66	-7.91	-5.67	-0.36
	2	-126.31	-109.69	-64.67	-61.12	-50.29	-19.87	-41.67	-33.64	-9.58	-24.19	-18.71	-0.85
	3	-63.81	-44.66	2.18	-120.16	-96.45	-35.54	-75.42	-59.33	-14.07	-44.87	-34.38	-1.17
	4	-115.25	-80.04	-6.77	-185.87	-142.55	-47.07	-111.95	-84.29	-16.52	-68.33	-50.74	-1.07
	5	-217.33	-150.52	-33.48	-265.54	-193.78	-60.08	-150.90	-107.99	-18.31	-93.75	-66.85	-0.97
L=.20	1	-6.17	-5.19	-2.69	-4.94	-4.07	-1.81	-3.66	-2.94	-1.07	-2.08	-1.54	-0.11
	2	-22.14	-19.70	-10.21	-16.46	-14.35	-6.00	-12.01	-10.32	-3.46	-6.73	-5.49	-0.32
	3	-50.68	-45.63	-24.43	-32.83	-28.78	-11.33	-23.61	-20.46	-6.28	-13.38	-11.15	-0.57
	4	-88.68	-79.30	-41.17	-52.27	-45.36	-16.30	-37.30	-32.08	-8.72	-21.58	-17.99	-0.70
	5	-146.50	-129.69	-66.70	-75.87	-64.89	-22.01	-52.96	-44.92	-11.03	-31.15	-25.78	-0.86
L=.40	1	-1.46	-1.23	-0.59	-1.25	-1.04	-0.46	-0.93	-0.76	-0.28	-0.53	-0.39	-0.03
	2	-5.12	-4.58	-2.21	-4.28	-3.79	-1.65	-3.16	-2.76	-0.99	-1.74	-1.44	-0.09
	3	-10.89	-9.92	-4.82	-8.81	-7.95	-3.37	-6.48	-5.78	-2.00	-3.57	-3.05	-0.18
	4	-18.34	-16.78	-7.94	-14.56	-13.19	-5.32	-10.70	-9.60	-3.13	-5.94	-5.14	-0.26
	5	-28.26	-25.89	-12.24	-21.61	-19.58	-7.60	-15.85	-14.23	-4.43	-8.88	-7.71	-0.36
L=1.0	1				-0.20	-0.17	-0.07	-0.15	-0.12	-0.05	-0.08	-0.06	0.00
	2				-0.69	-0.62	-0.27	-0.51	-0.45	-0.16	-0.28	-0.23	-0.02
	3				-1.45	-1.32	-0.58	-1.07	-0.97	-0.35	-0.58	-0.50	-0.03
	4				-2.45	-2.25	-0.96	-1.81	-1.64	-0.58	-0.98	-0.86	-0.05
	5				-3.71	-3.43	-1.45	-2.74	-2.50	-0.87	-1.49	-1.32	-0.07

Note: Percent error for each beam theory as compared to elasticity solutions are given for the anisotropic graphite magnesium for the first five flexural modes of vibration. EB = Euler-Bernoulli, Ray = Rayleigh, Timo = Timoshenko
 Green-shaded cells have error within 5 percent of elasticity solutions, blue-shaded cells have error between 5 and 50 percent, red shaded cells have error in excess of 50 percent

Table 12. Percent Error from Elasticity Solutions (Isotropic)

Beam Length (m)	Flexural Mode Number	Wall Thickness (m)											
		0.0005			0.001			0.002			0.004		
		EB	Ray	Timo	EB	Ray	Timo	EB	Ray	Timo	EB	Ray	Timo
L=.01	1	-589.07	-134.61	-18.87	-273.74	-32.90	30.94	-262.63	-39.83	23.41	-158.11	-11.34	33.55
	2	-1220.65	-225.67	-20.89	-964.79	-174.51	-1.93	-502.83	-68.95	37.21	-317.31	-31.54	51.01
	3	-1753.23	-260.56	-25.01	-1219.82	-168.97	5.86	-714.41	-81.11	35.35	-571.72	-68.97	37.67
	4	-2522.00	-316.32	-18.09	-1384.73	-147.20	29.76	-934.33	-88.34	46.27	-991.94	-125.76	35.14
	5	-2694.28	-273.80	-12.91	-1830.50	-170.96	18.02	-1314.05	-117.35	34.00	-1161.12	-120.59	32.58
L=.02	1	-126.33	-33.01	-5.20	-187.32	-74.33	-38.28	-92.70	-23.83	1.14	-61.58	-11.89	9.61
	2	-426.56	-134.16	5.11	-458.22	-157.90	-9.04	-314.28	-105.36	5.82	-176.09	-50.64	22.81
	3	-774.10	-216.48	-30.88	-708.99	-205.14	-27.55	-503.17	-145.51	-5.13	-275.53	-69.81	23.81
	4	-995.70	-231.42	-1.75	-870.21	-206.45	4.21	-863.21	-229.87	-6.86	-504.19	-131.58	20.84
	5	-1490.90	-311.33	-30.57	-1014.72	-201.45	3.61	-967.18	-213.96	-2.05	-746.98	-180.38	5.97
L=.05	1	-54.23	-35.26	-18.89	-29.24	-14.60	-1.45	-21.24	-9.53	1.76	-13.86	-5.17	3.99
	2	-211.18	-141.39	-73.16	-86.70	-47.62	-7.56	-56.48	-27.89	4.13	-35.49	-15.34	10.16
	3	-434.33	-266.85	-129.82	-173.23	-92.36	-22.43	-97.22	-45.18	4.81	-60.69	-25.18	14.36
	4	-606.51	-331.08	-123.69	-260.82	-126.78	-22.29	-146.12	-63.17	6.64	-89.38	-34.60	18.07
	5	-813.75	-398.95	-132.54	-362.49	-161.04	-25.82	-202.16	-81.12	6.48	-121.39	-43.74	20.23
L=.10	1	-10.05	-6.16	-1.16	-7.85	-4.38	0.15	-5.98	-3.13	0.69	-3.79	-1.64	1.35
	2	-34.31	-24.45	-7.31	-23.08	-14.81	0.01	-17.03	-10.40	2.12	-10.45	-5.57	4.26
	3	-84.46	-62.88	-26.66	-44.26	-28.72	-1.52	-31.41	-19.36	3.41	-19.24	-10.61	7.37
	4	-148.58	-107.93	-46.86	-69.38	-43.71	-3.20	-47.88	-28.58	4.78	-29.59	-16.05	10.35
	5	-249.48	-175.89	-79.31	-101.64	-62.05	-7.19	-66.44	-37.98	5.65	-41.21	-21.61	12.87
L=.20	1	-2.36	-1.42	-0.04	-2.02	-1.17	0.09	-1.55	-0.85	0.20	-0.97	-0.44	0.37
	2	-7.48	-5.33	-0.37	-6.13	-4.21	0.30	-4.63	-3.05	0.72	-2.78	-1.59	1.32
	3	-15.59	-11.71	-1.64	-12.05	-8.64	0.43	-9.00	-6.22	1.39	-5.35	-3.28	2.63
	4	-26.22	-19.95	-3.48	-19.37	-13.96	0.64	-14.39	-10.04	2.26	-8.59	-5.39	4.19
	5	-41.56	-31.91	-7.68	-28.25	-20.25	0.52	-20.78	-14.44	3.06	-12.47	-7.86	5.82
L=.40	1	-0.58	-0.35	0.01	-0.51	-0.30	0.03	-0.39	-0.22	0.05	-0.24	-0.11	0.09
	2	-1.82	-1.30	0.02	-1.57	-1.10	0.10	-1.19	-0.80	0.20	-0.71	-0.41	0.35
	3	-3.70	-2.80	-0.01	-3.13	-2.32	0.21	-2.36	-1.69	0.41	-1.38	-0.87	0.74
	4	-6.16	-4.76	-0.05	-5.16	-3.90	0.37	-3.87	-2.84	0.73	-2.26	-1.48	1.26
	5	-9.33	-7.31	-0.26	-7.68	-5.87	0.52	-5.74	-4.27	1.08	-3.35	-2.24	1.88
L=1.0	1	-0.09	-0.06	0.00	-0.08	-0.05	0.00	-0.06	-0.04	0.01	-0.04	-0.02	0.02
	2	-0.29	-0.21	0.01	-0.25	-0.18	0.02	-0.19	-0.13	0.03	-0.11	-0.07	0.06
	3	-0.58	-0.44	0.02	-0.51	-0.38	0.04	-0.38	-0.28	0.07	-0.22	-0.14	0.12
	4	-0.97	-0.76	0.04	-0.84	-0.65	0.07	-0.63	-0.47	0.13	-0.37	-0.24	0.22
	5	-1.47	-1.16	0.06	-1.27	-0.99	0.11	-0.95	-0.72	0.20	-0.55	-0.37	0.33

Note: Percent error for each beam theory as compared to elasticity solutions are given for the isotropic steel for the first five flexural modes of vibration. EB = Euler-Bernoulli, Ray = Rayleigh, Timo = Timoshenko
 Green-shaded cells have error within 5 percent of elasticity solutions, blue-shaded cells have error between 5 and 50 percent, red shaded cells have error in excess of 50 percent

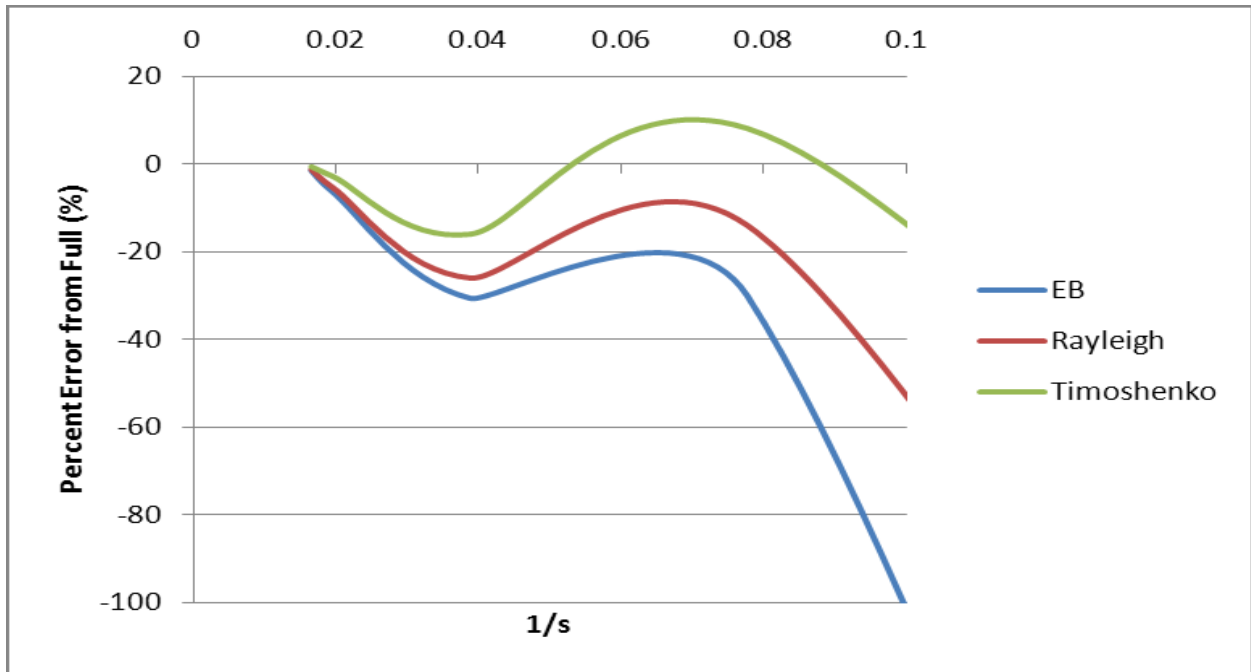


Figure 1. Mode 1 Percent Error from Elasticity--Wall Thickness 0.0005 m

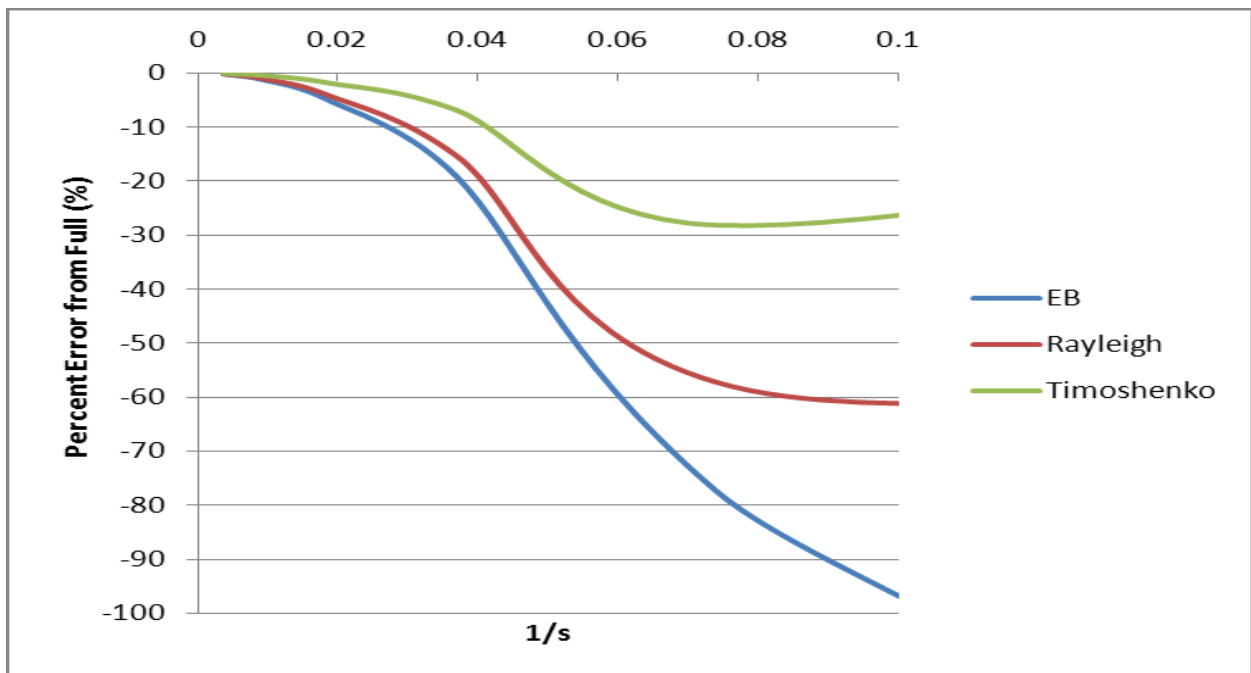


Figure 2. Mode 1 Percent Error from Elasticity--Wall Thickness 0.001 m

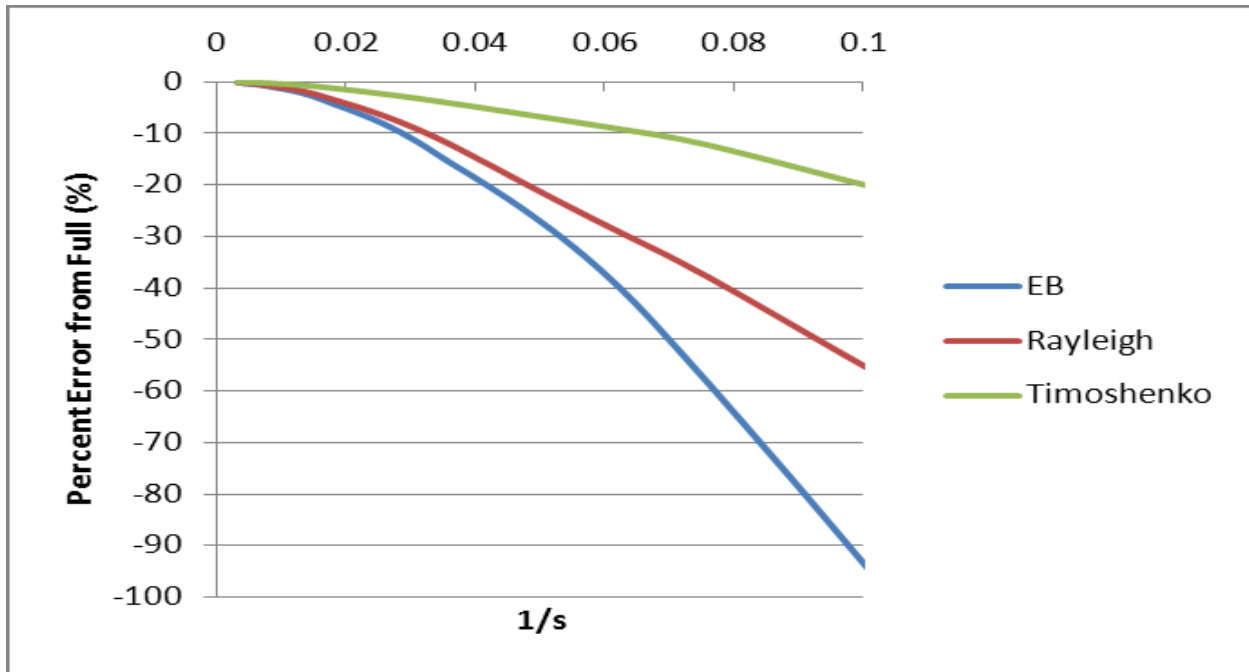


Figure 3. Mode 1 Percent Error from Elasticity--Wall Thickness 0.002 m

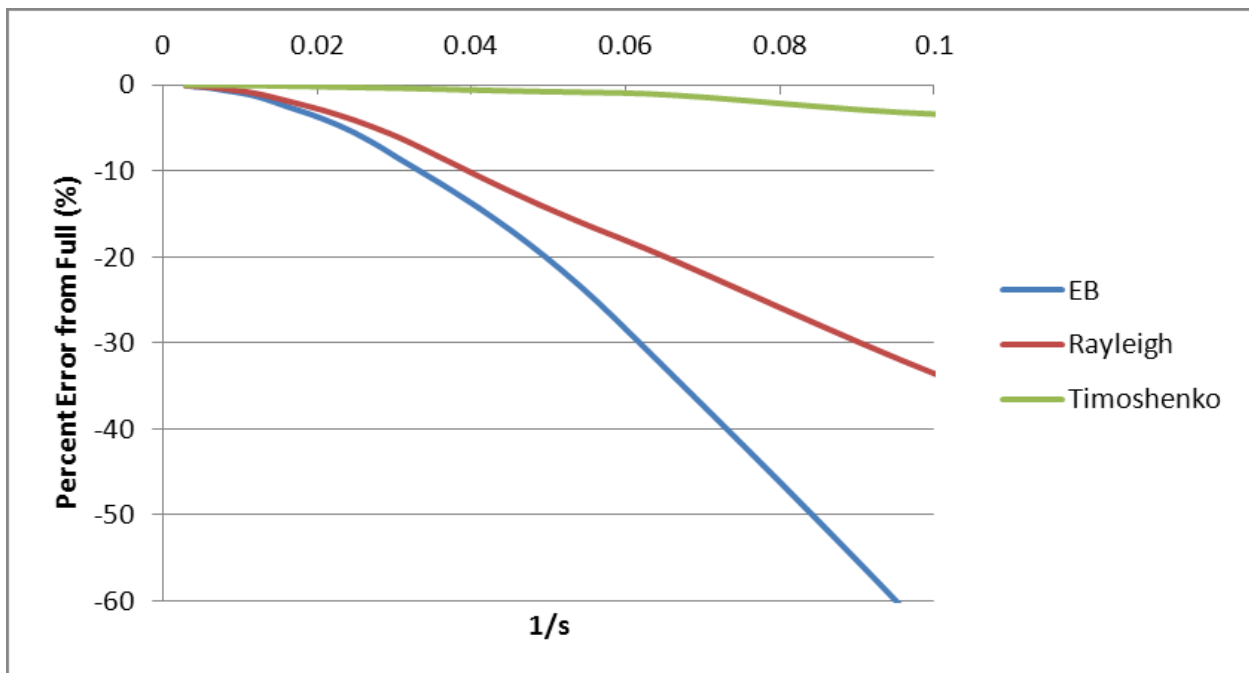


Figure 4. Mode 1 Percent Error from Elasticity--Wall Thickness 0.004 m

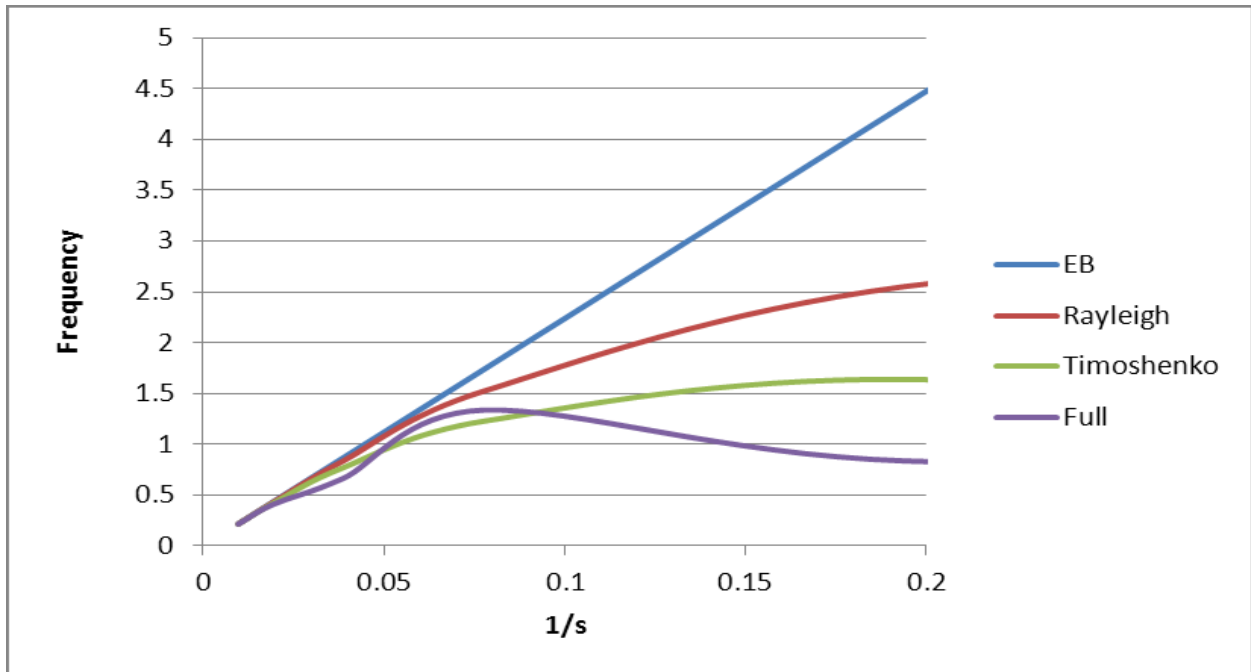


Figure 5. Scaled Mode 1 Frequencies--Wall Thickness 0.0005 m

Note: The dimensionless natural frequencies are scaled by the factor $L \frac{\rho}{E}$

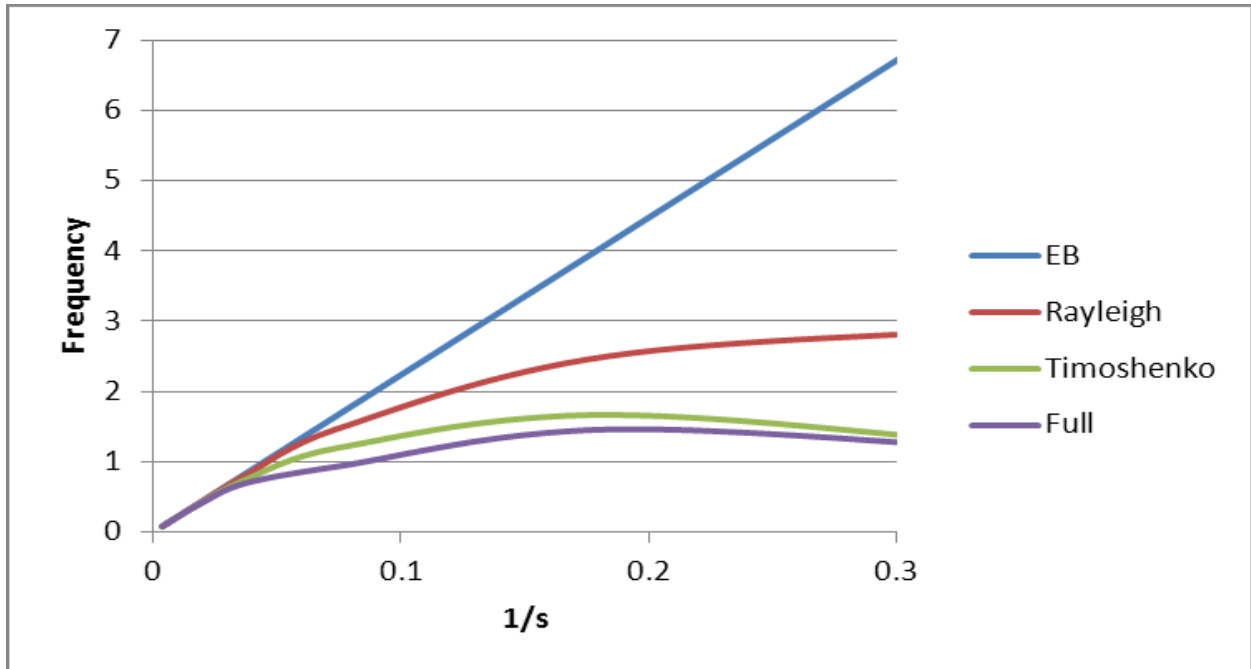


Figure 6. Scaled Mode 1 Frequencies--Wall Thickness 0.001 m

Note: The dimensionless natural frequencies are scaled by the factor $L \frac{\rho}{E}$

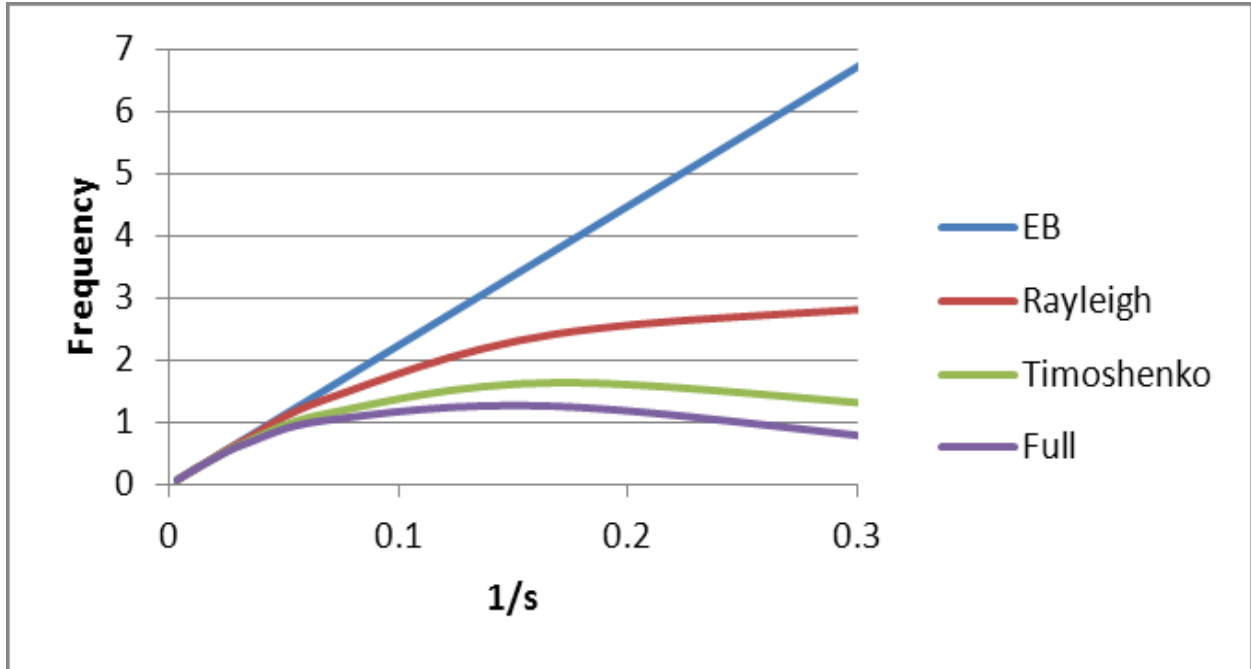


Figure 7. Scaled Mode 1 Frequencies--Wall Thickness 0.002 m

Note: The dimensionless natural frequencies are scaled by the factor $L \frac{\rho}{E}$

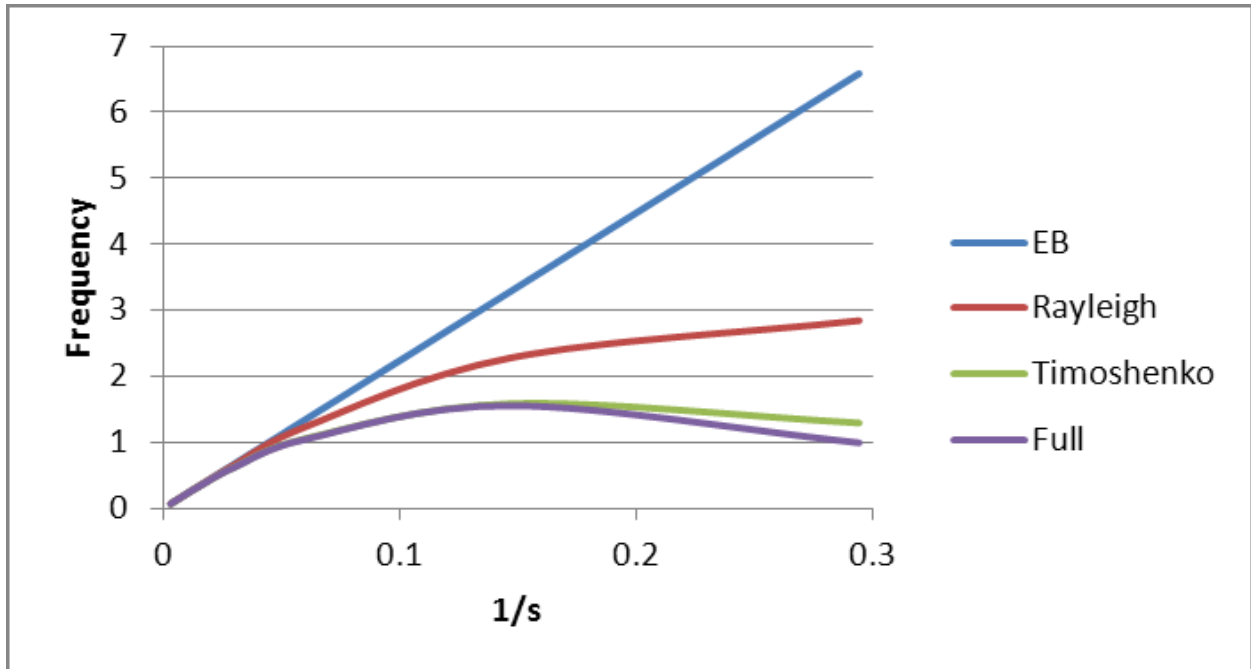


Figure 8. Scaled Mode 1 Frequencies--Wall Thickness 0.004 m

Note: The dimensionless natural frequencies are scaled by the factor $L \frac{\rho}{E}$

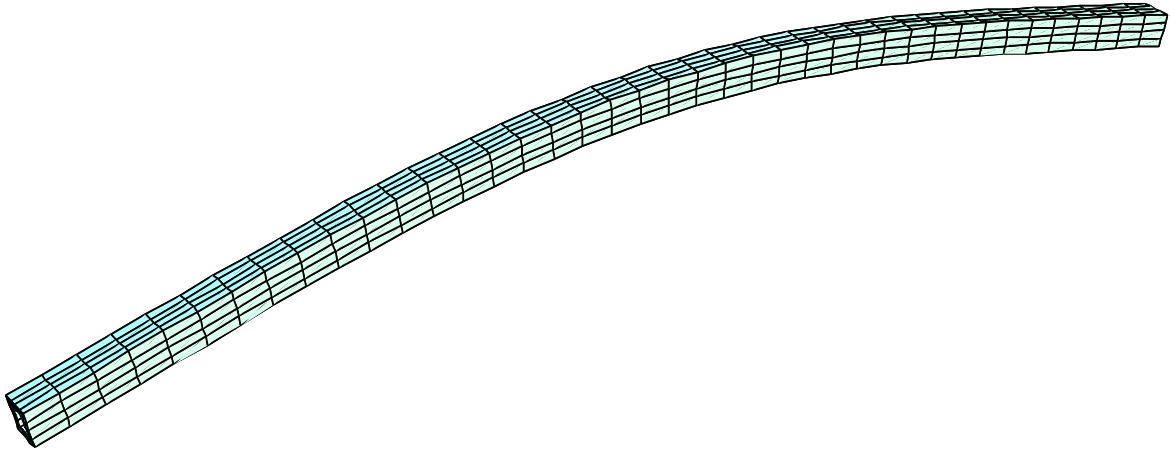


Figure 9. Mode 1 Deformation--Length of 0.20 m

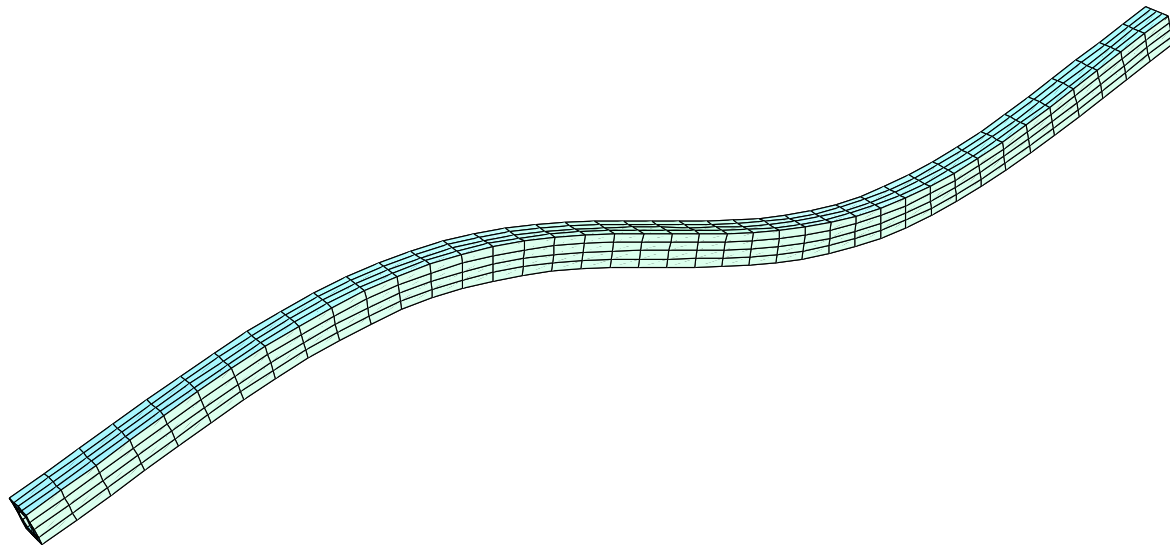


Figure 10. Mode 2 Deformation--Length of 0.20 m

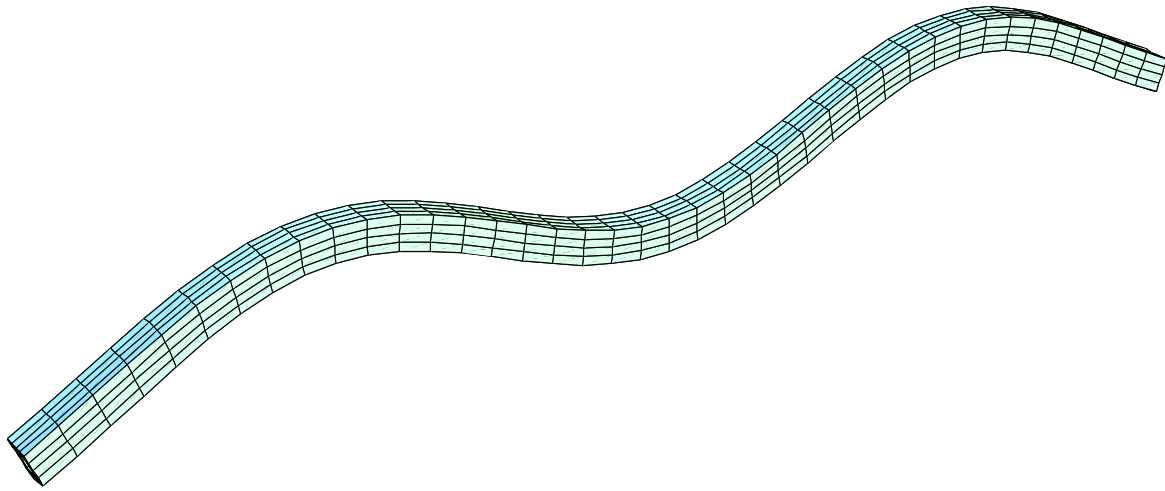


Figure 11. Mode 3 Deformation--Length of 0.20 m

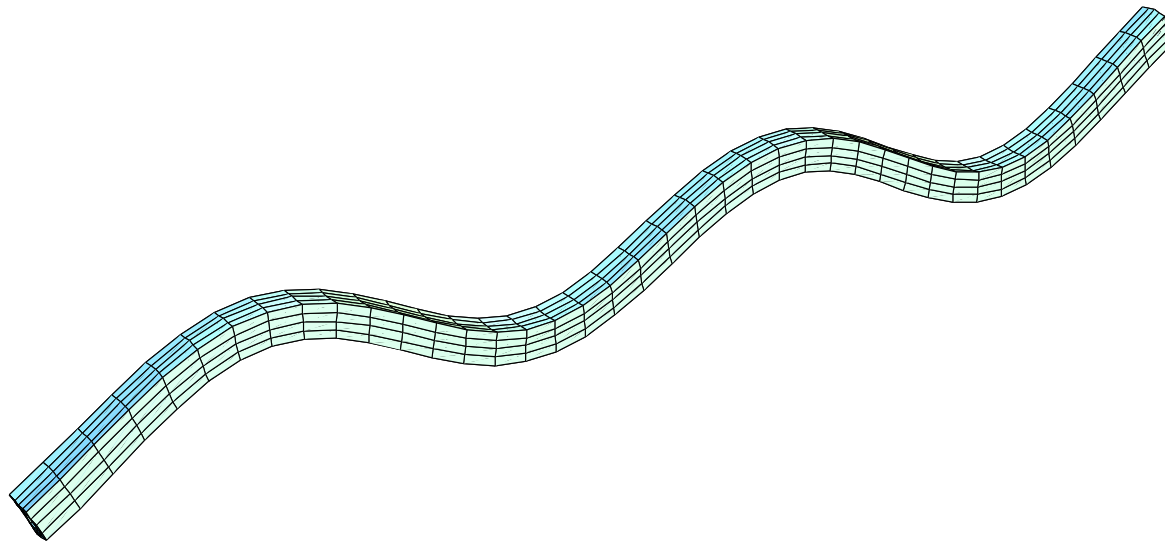


Figure 12. Mode 4 Deformation--Length of 0.20 m

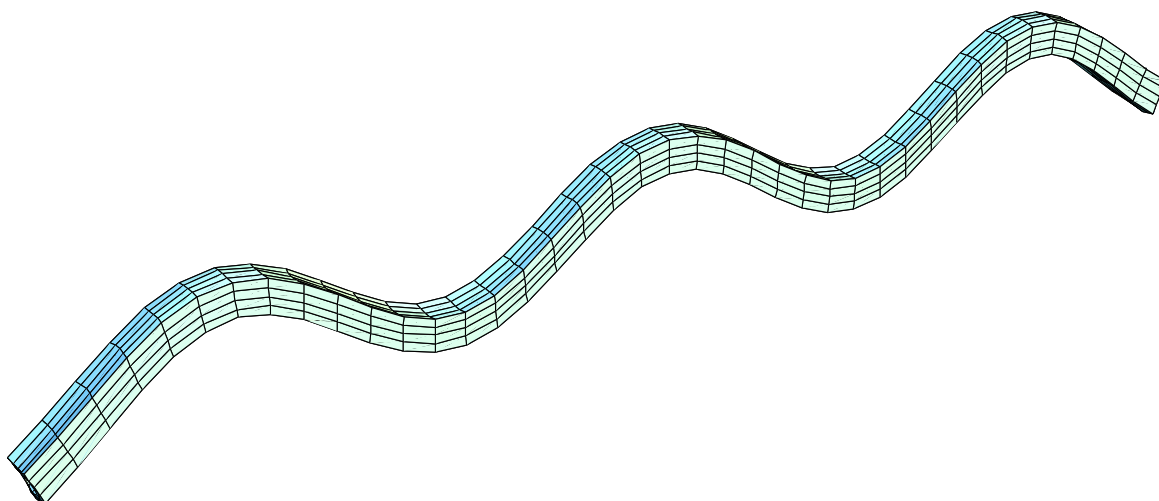


Figure 13. Mode 5 Deformation--Length of 0.20 m

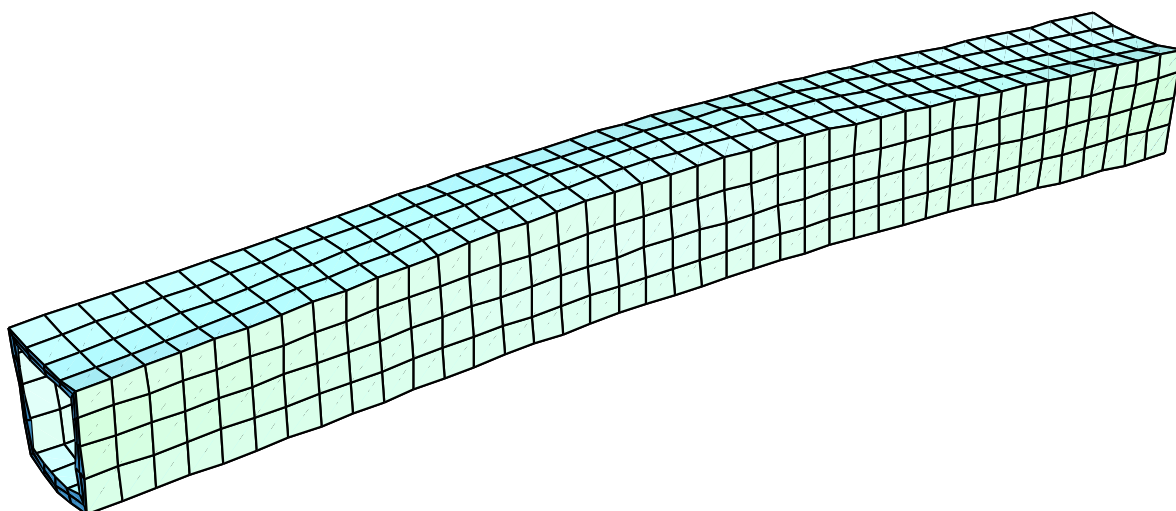


Figure 14. Mode 1 Deformation--Length of 0.05 m

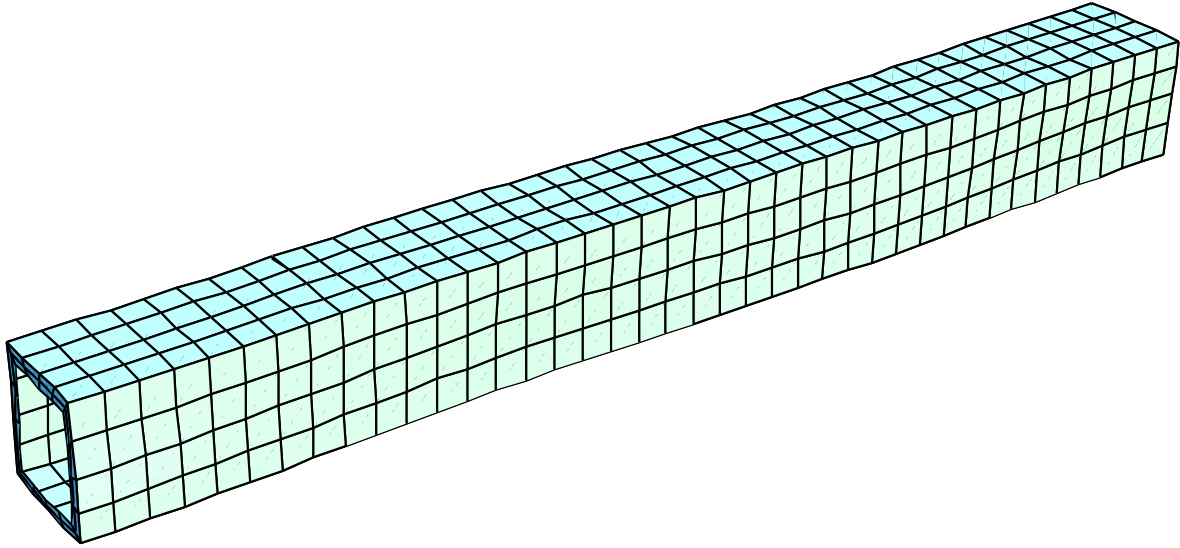


Figure 15. Mode 2 Deformation--Length of 0.05 m

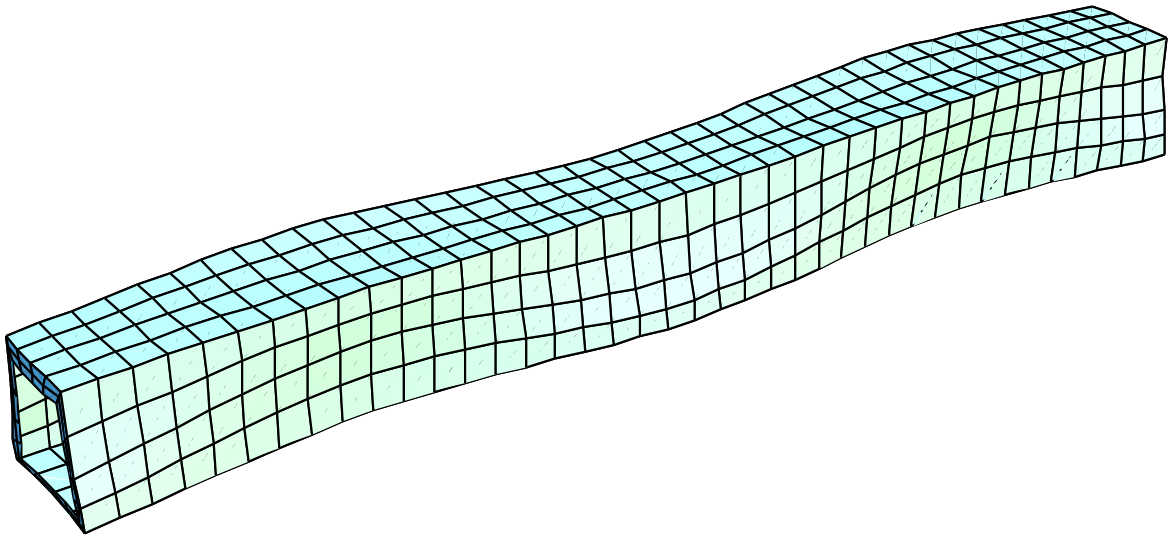


Figure 16. Mode 3 Deformation--Length of 0.05 m

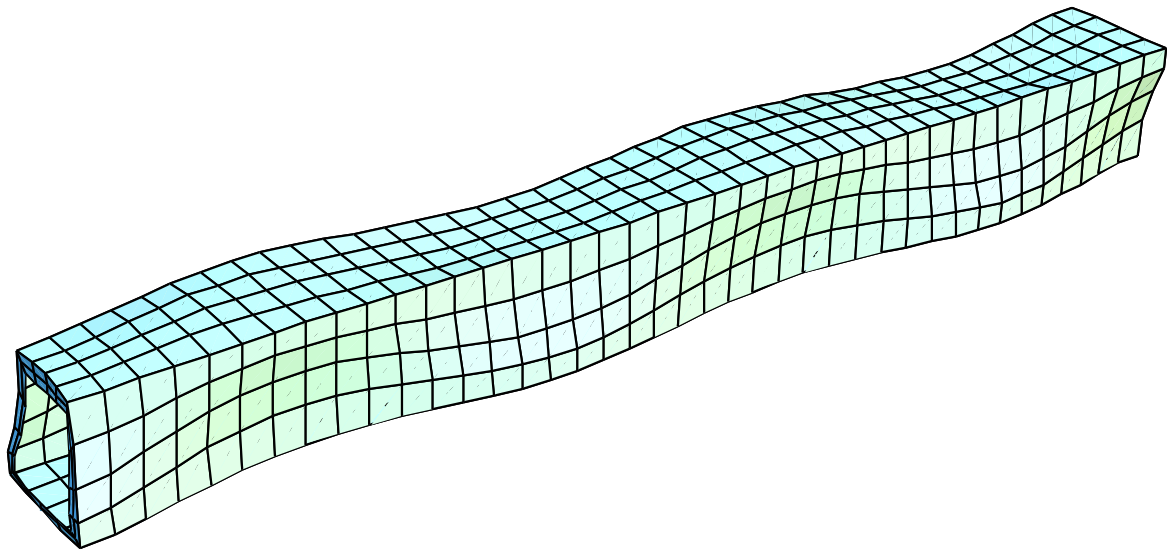


Figure 17. Mode 4 Deformation--Length of 0.05 m

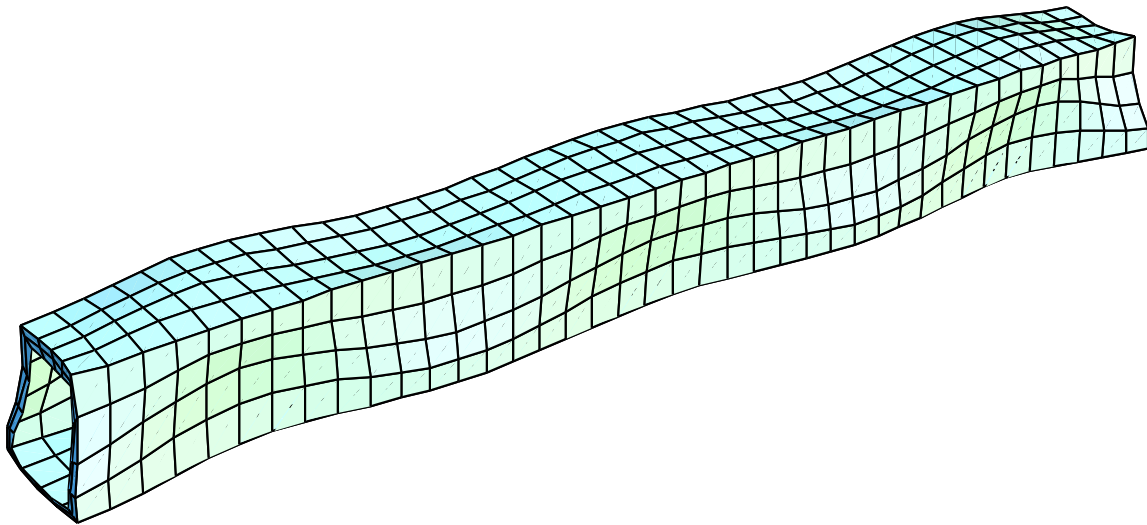


Figure 18. Mode 5 Deformation--Length of 0.05 m

Table 13. Mode 1 Deformed Cross-Sections

Wall Thickness (m)	Beam Length (m)		
	0.05	0.10	0.20
0.0005			
0.001			
0.002			
0.004			

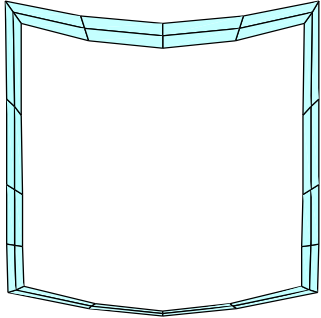
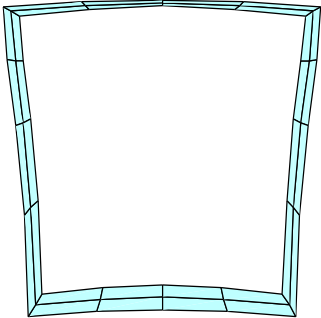
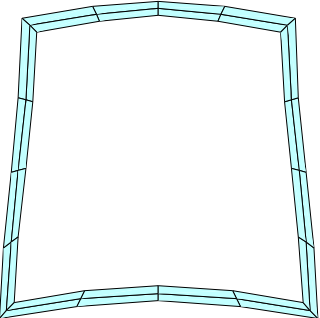
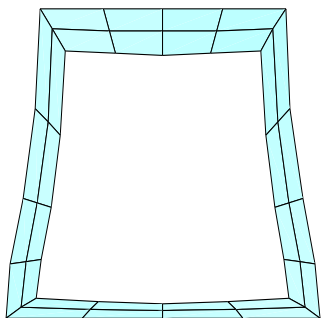
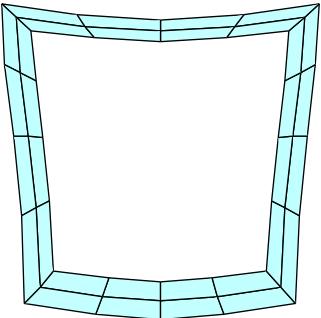
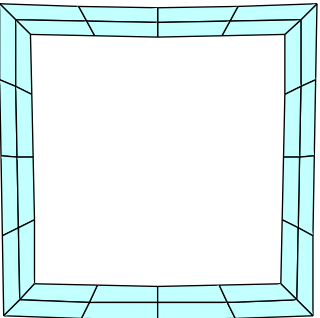
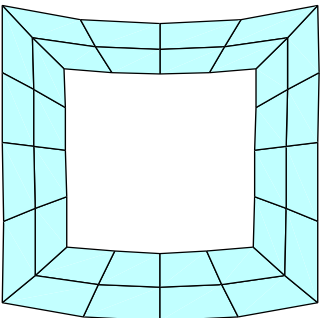
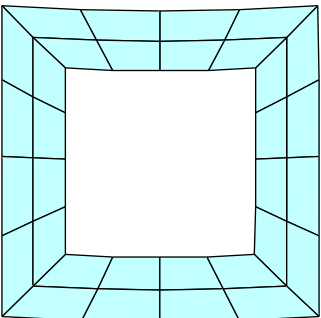
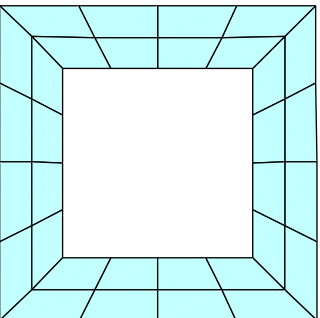
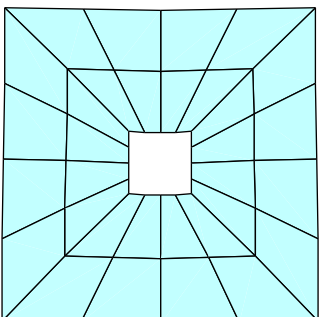
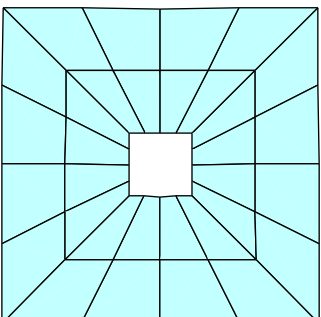
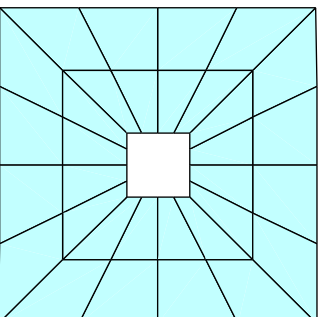
Note: The outside dimensions of each cross-section are 0.01 m X 0.01 m. The deformed shapes are for the anisotropic graphite-magnesium

Table 14. Mode 2 Deformed Cross-Sections

Wall Thickness (m)	Beam Length (m)		
	0.05	0.10	0.20
0.0005			
0.001			
0.002			
0.004			

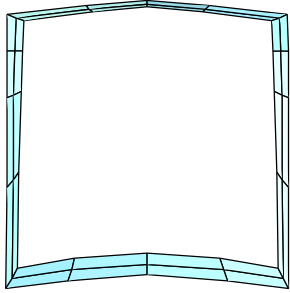
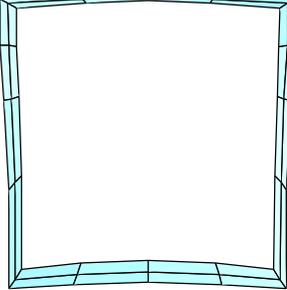
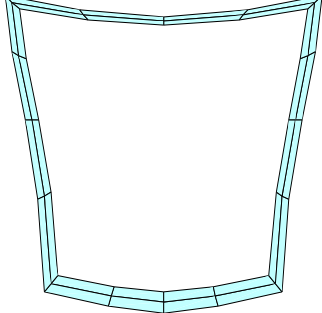
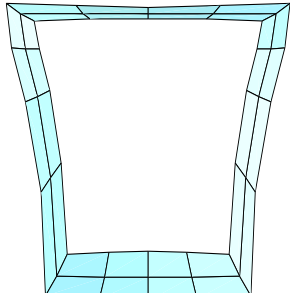
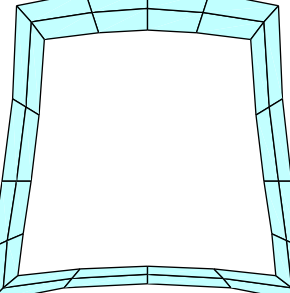
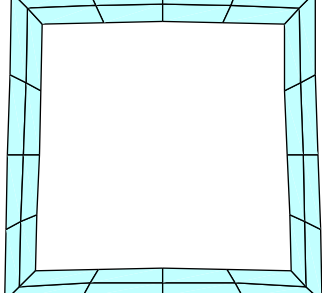
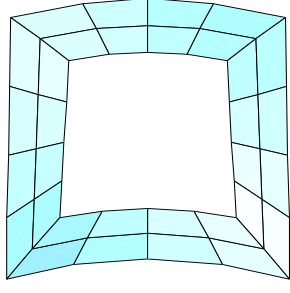
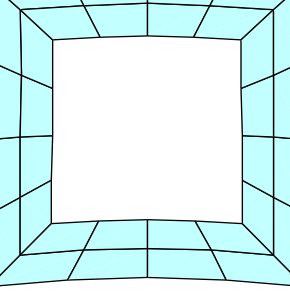
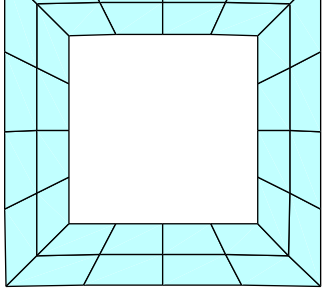
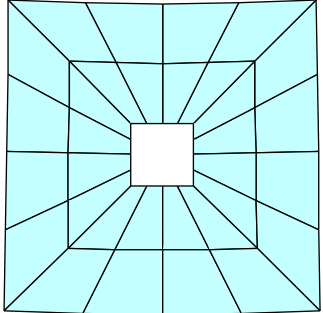
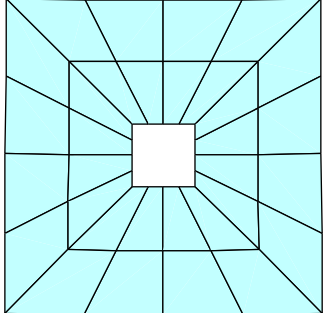
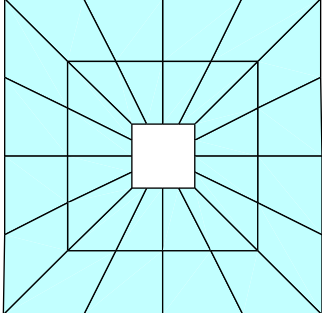
Note: The outside dimensions of each cross-section are 0.01 m X 0.01 m. The deformed shapes are for the anisotropic graphite-magnesium

Table 15. Mode 3 Deformed Cross-Sections

Wall Thickness (m)	Beam Length (m)		
	0.05	0.10	0.20
0.0005			
0.001			
0.002			
0.004			

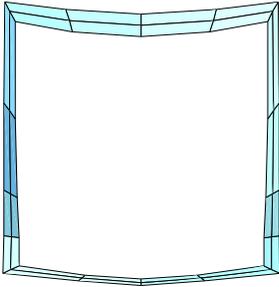
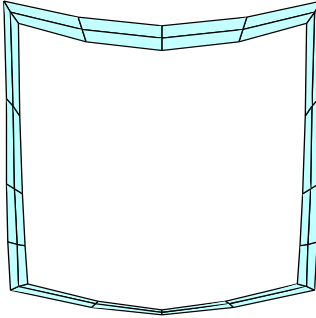
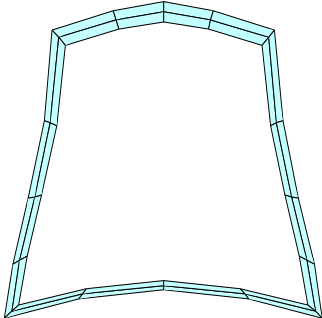
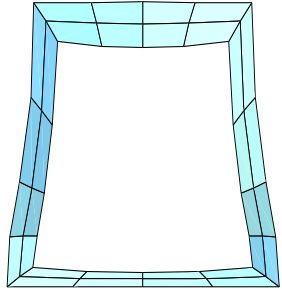
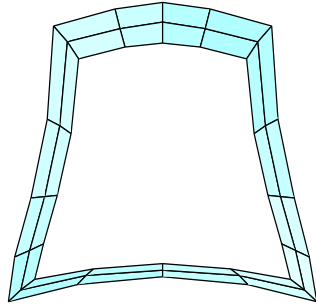
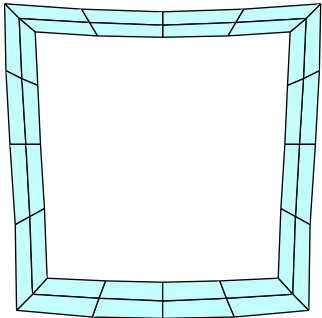
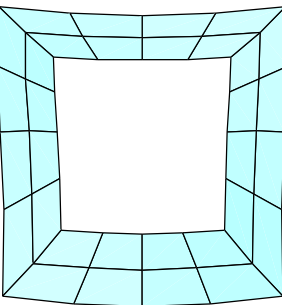
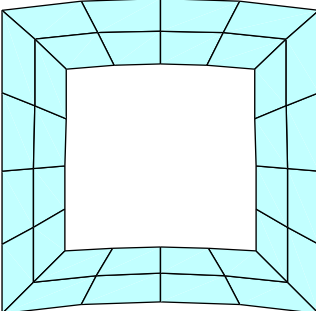
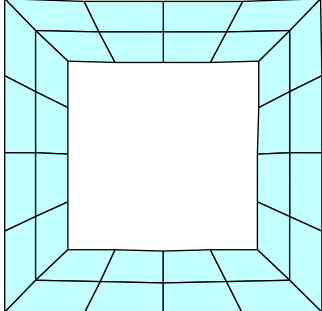
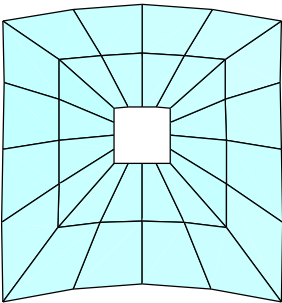
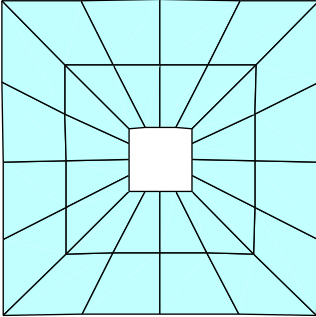
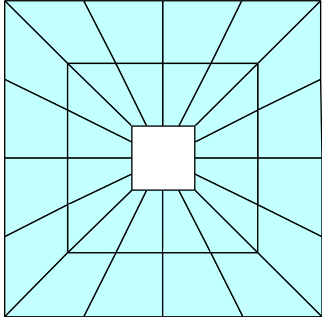
Note: The outside dimensions of each cross-section are 0.01 m X 0.01 m. The deformed shapes are for the anisotropic graphite-magnesium

Table 16. Mode 4 Deformed Cross-Sections

Wall Thickness (m)	Beam Length (m)		
	0.05	0.10	0.20
0.0005			
0.001			
0.002			
0.004			

Note: The outside dimensions of each cross-section are 0.01 m X 0.01 m. The deformed shapes are for the anisotropic graphite-magnesium

Table 17. Mode 5 Deformed Cross-Sections

Wall Thickness (m)	Beam Length (m)		
	0.05	0.10	0.20
0.0005			
0.001			
0.002			
0.004			

Note: The outside dimensions of each cross-section are 0.01 m X 0.01 m. The deformed shapes are for the anisotropic graphite-magnesium

Chapter 5

Conclusions

Section 5.1: Anisotropic Beams

The slenderness ratio is certainly the key to the accuracy of the approximate beam theories. As the slenderness ratio increases, accuracy in predicting the natural frequencies of vibration increases as well. This result begs the question: At what point does it become prudent to use one beam theory over another? For very slender anisotropic beams with a slenderness ratio of 270.5 or more, each of the three approximate beam theories is accurate to within 4 % for the first five modes of vibration. When the slenderness ratio is at least 108.2, each of the beam theories is accurate to within 5 % for just the first two modes of vibration. When the slenderness ratio is at least 54.1, each of the beam theories is still within 5 % error, but only for the first mode of vibration. See Table 22 in the Appendix for a listing of the slenderness ratios for each beam length and wall thickness combination.

As other researchers have pointed out and as was confirmed in this study, the Timoshenko beam theory is without question the most accurate predictor of natural frequencies as far as approximate methods are concerned. In regards to the first mode of vibration, it is recommended that only the Timoshenko model be used to approximate the natural frequencies for hollow anisotropic beams with slenderness ratios below 54.1. As the slenderness ratio dips below this level, the percent error for the Euler-Bernoulli and Rayleigh models exceed 5 %. In some cases

the Timoshenko model is accurate to within 1.9 % for a slenderness ratio as low as 6.8.

However, another beam with a slenderness ratio of 13.5 produced a natural frequency that was over 28 % higher than the full elasticity solutions. For every case with a slenderness ratio greater than 29.7, the Timoshenko model gave natural frequencies under 3.7 % error for the lowest mode of vibration. With this in mind, it is recommended that only three-dimensional elasticity solutions be used to calculate the natural frequencies for hollow anisotropic beams with a slenderness ratio below 29.7.

For hollow beams with slenderness ratios above 60.4, the Rayleigh beam theory provides an improvement over the Euler-Bernoulli beam theory of as little as 0.02 % and as much as 4.3 %. Over the same range of slenderness ratios, the Timoshenko beam theory provides an improvement over the Euler-Bernoulli beam theory of between 0.08 % and 30.0 %. Knowing this, it seems impractical to ever use the Rayleigh beam theory. If accuracy is of significant concern, the Timoshenko beam theory provides much more improvement from the Euler-Bernoulli theory than does the Rayleigh theory. Given that the Rayleigh theory is also more complex than the Euler-Bernoulli theory, this conclusion is reinforced even further. The rotary inertia term used in the Rayleigh method can also be incorporated into the mass matrix in finite element formulations that are commonly used to solve such problems. Thus, it is clear the Rayleigh beam theory provides limited resourcefulness as compared to the Euler-Bernoulli and Timoshenko models.

As stated previously, the Euler-Bernoulli method provides natural frequencies within 4 % of exact solutions for slenderness ratios above 270.5 up to the fifth mode of vibration. Since higher modes of vibration are very unlikely to be excited, even for such slender structures, it is recommended that the Euler-Bernoulli model be used with slenderness ratios beyond 270.5.

Even on the chance that the higher order modes are excited, their contribution to the total deformation is very small.

For hollow beams with slenderness ratios above 67.9, the Timoshenko theory produced natural frequencies up to the fifth mode of vibration that were within 5 % of elasticity solutions with only one exception. At a slenderness ratio of 108.2, the natural frequencies for the fourth and fifth modes were within 7.6 %. Because the higher order modes of vibrations are unlikely to be excited in beams with such low slenderness ratios, the Timoshenko model proves to be adequate in this range. In calculating natural frequencies for modes of vibration higher than mode one, the full elasticity solutions are recommended for slenderness ratios below 67.9. Above a slenderness ratio of 67.9, the Timoshenko model is accurate to within 5.3 % for the first four modes of vibration. Table 18 provides a summary of the recommended situations in which the respective beam theories are satisfactory for anisotropic beams.

Table 18. Suggested Uses of Beam Theories (Anisotropic)

Slenderness Ratio	Modes of Vibration				
	1	2	3	4	5
0-29.7	Elasticity	Elasticity	Elasticity	Elasticity	Elasticity
29.7-67.9	Timoshenko	Elasticity	Elasticity	Elasticity	Elasticity
67.9-108.2	Timoshenko	Timoshenko	Timoshenko	Timoshenko	Timoshenko
108.2-270.5	Euler-Bernoulli	Euler-Bernoulli	Timoshenko	Timoshenko	Timoshenko
above 270.5	Euler-Bernoulli	Euler-Bernoulli	Euler-Bernoulli	Euler-Bernoulli	Euler-Bernoulli

Section 5.2: Isotropic Beams

For isotropic beams with a slenderness ratio of 135.9 or more, each of the beam theories is accurate to within 3.4 % for the first five modes of vibration. In some instances with the isotropic beams, beam theories are accurate to within 3.7 % for the first three modes of vibration

when the slenderness ratio is at least 60.4, however there are a few exceptions. When the slenderness ratio drops below 13, none of the beam theories are accurate for the isotropic case.

As was the case for the anisotropic beams, the Timoshenko model is clearly the most accurate in calculating natural frequencies for isotropic beams. For the first mode of vibration, the Timoshenko theory is accurate to within 1.5 % for most instances with a slenderness ratio down to 13.5. It is recommended that for slenderness ratios ranging between 13.5 and 27.1, the Timoshenko model be used for the first mode of vibration for hollow isotropic beams. Below this level, errors ranged as high as 38 %. As such, only the elasticity solutions should be used to calculate natural frequencies for the isotropic beams below 13.5. Elasticity solutions should also be used for the second mode of vibration and beyond when the slenderness ratio is between 13.5 and 27.1. For slenderness ratios between 27.1 and 135.9, the Timoshenko model is recommended for the first four modes of vibration. In this range, the Timoshenko theory is accurate to within 4.8 % for nearly every case. For isotropic beams with slenderness ratios above 135.9, the Euler-Bernoulli method is recommended for the first five modes, as it is accurate to within 3.4 % of elasticity solutions.

For isotropic beams with a slenderness ratio of at least 51.5, the Rayleigh beam theory provides an improvement over the Euler-Bernoulli beam theory that ranges between 0.02 % and 6.8 %. The Timoshenko theory provides an improvement over the Euler-Bernoulli model of 0.05 % to 23.9 % for the same range of slenderness ratios. Similar to the anisotropic case, the Rayleigh model proves to be of limited resourcefulness. While it provides a better representation of the true natural frequencies as compared to the Euler-Bernoulli model, the improvement is insignificant given the more complex nature of the calculations. For a similarly complex formulation, the Timoshenko model provides much greater improvement over the Euler-

Bernoulli model. As mentioned in the discussion of the anisotropic results, the rotary inertia term can be included in the mass matrix of finite element formulations if desired. Thus, the Rayleigh beam theory is not recommended for calculating the natural frequencies. Table 19 provides a summary of suggested uses of beam theories for isotropic beams.

Table 19. Suggested Uses of Beam Theories (Isotropic)

Slenderness Ratio	Modes of Vibration				
	1	2	3	4	5
0-13.5	Elasticity	Elasticity	Elasticity	Elasticity	Elasticity
13.5-27.1	Timoshenko	Elasticity	Elasticity	Elasticity	Elasticity
27.1-135.9	Timoshenko	Timoshenko	Timoshenko	Timoshenko	Elasticity
above 135.9	Euler-Bernoulli	Euler-Bernoulli	Euler-Bernoulli	Euler-Bernoulli	Euler-Bernoulli

When comparing the accuracy of beam theories for the anisotropic and isotropic conditions, it is clear that more error is introduced for the anisotropic case. The only constants that changed when moving from anisotropic to isotropic were the density, the components of the elastic stiffness tensor, and the shape factor. The shear modulus for the isotropic steel is smaller relative to the modulus of elasticity as compared to the relative size of the shear modulus to the elastic modulus of the graphite-magnesium. This will introduce greater error for the Timoshenko model in evaluating the anisotropic beams. The density for the isotropic steel is also much greater than the density of the anisotropic graphite-magnesium. As a result, the frequencies themselves will be reduced significantly for the isotropic beams. In referring back to Tables 3 through 10, this trend is evident. In most instances the anisotropic frequencies are double the frequencies of the isotropic steel for beams with the same slenderness ratios. As discussed earlier, much greater accuracy is introduced at lower frequencies. This provides logical reasoning for the reduced

accuracy of the beam theories in calculating natural frequencies for anisotropic beams as compared to the isotropic beams.

Section 5.3: Shape Factor

To assess the validity of using a single shape factor for all square, hollow anisotropic beams with the Timoshenko theory, an iterative calculation method to find the shape factor was introduced. Initially, the lowest natural frequency for each beam length and wall thickness combination was forced to match the natural frequency calculated by elasticity methods by using an iterative process that altered the shape factor. Then, using this new shape factor, the higher order natural frequencies were determined for each case. Table 20 shows a comparison of the error in determining the natural frequencies using the Timoshenko model with a fixed shape factor of 0.8442 and a shape factor determined by matching the lowest natural frequency. It is clear that error in determining the subsequent natural frequencies is significantly reduced when a shape factor that comes from matching the lowest natural frequency is used. In some cases, an improvement of nearly 4700 times is evident for higher order modes. This leads one to question the validity of using Pucheggar's proposed method for determining the shape factor as it applies to hollow anisotropic beams. Clearly, the absolute dimensions of the wall thicknesses have to be considered, not only the outside dimensions of the beam. In the determination of the shape factor, the cross-sectional area and the moment of inertia should take into consideration the wall thickness as well. While Omidvar's formulation of the shape factor for thin-walled orthotropic laminated composite sections does take into account the wall thicknesses, it only considers their ratio, not the absolute dimensions [7]. Therefore, the shape factor would be the same for a beam

with walls 0.002 m thick as one with walls 0.004 m thick. In looking at Table 21 which displays the shape factors found by matching the lowest natural frequencies, one can see that this is not true. Table 21 shows that as the wall thickness increases, the shape factor increases, leaving much room for improvement. As Table 20 demonstrates, there are still several cases in which the error ranges between 50 % and 128 % for higher order modes of vibration, even when the lowest frequency is fixed to exact solutions. The only adjustment that can be made to the Timoshenko beam theory to correct this error is to alter the shape factor. This indicates that the shape factor is also dependent on the mode number, not just the beam cross-section.

Table 20. Percent Error from Elasticity Solutions Using Adjusted Shape Factor

Beam Length (m)	Flexural Mode Number	Wall Thickness (m)							
		0.0005		0.001		0.002		0.004	
		0.8442	Matching	0.8442	Matching	0.8442	Matching	0.8442	Matching
L=.01	1	-21.18	0.00	-4.02	0.00	8.22	0.00	26.25	0.00
	2	-53.87	-16.01	-9.84	-22.29	21.18	-38.35	-44.95	-14.64
	3	-48.48	4.32	5.80	-3.50	18.88	-65.11	20.18	-75.42
	4	-12.40	-2.63	16.96	-32.65	27.99	-100.49	-5.28	-93.43
	5	24.68	-22.93	24.30	-41.57	31.46	-86.41	16.97	-82.21
L=.02	1	-96.12	0.00	-14.14	0.00	-29.85	0.00	-1.88	0.00
	2	-51.05	-1.91	14.12	-0.74	9.77	-2.41	29.60	-0.96
	3	-101.31	-18.59	-5.20	-27.55	6.39	-55.62	17.29	-38.05
	4	-54.99	9.16	-17.62	-2.26	18.51	-62.29	27.85	-50.86
	5	-38.62	-12.49	-2.82	-19.77	43.47	-68.86	34.67	-49.22
L=.05	1	8.14	0.00	-28.15	0.00	-10.12	0.00	-0.90	0.00
	2	-20.40	-27.13	-0.23	-10.11	-18.74	0.47	-1.37	0.54
	3	-62.46	-79.56	-3.54	-53.25	-21.54	0.00	-1.01	1.28
	4	-53.89	-70.39	2.39	-63.19	-8.33	-1.16	-0.89	1.77
	5	-65.22	-76.78	-1.53	-70.73	-14.01	-17.05	0.80	-0.03
L=.10	1	-15.98	0.00	-6.89	0.00	-3.66	0.00	-0.36	0.00
	2	-64.67	-19.60	-19.87	-2.13	-9.58	0.16	-0.85	0.17
	3	2.18	-53.83	-35.54	-9.14	-14.07	0.17	-1.17	0.43
	4	-6.77	-89.43	-47.07	-13.97	-16.52	0.88	-1.07	0.96
	5	-33.48	-127.58	-60.08	-29.58	-18.31	1.12	-0.97	1.38
L=.20	1	-2.69	0.00	-1.81	0.00	-1.07	0.00	-0.11	0.00
	2	-10.21	-1.55	-6.00	-0.15	-3.46	0.07	-0.32	0.04
	3	-24.43	-8.42	-11.33	-0.90	-6.28	0.14	-0.57	0.11
	4	-41.17	-17.20	-16.30	-1.51	-8.72	0.54	-0.70	0.32
	5	-66.70	-33.20	-22.01	-3.25	-11.03	0.75	-0.86	0.49
L=.40	1	-0.59	0.00	-0.46	0.00	-0.28	0.00	-0.03	0.00
	2	-2.21	-0.09	-1.65	0.01	-0.99	0.02	-0.09	0.01
	3	-4.82	-0.56	-3.37	-0.03	-2.00	0.05	-0.18	0.03
	4	-7.94	-1.13	-5.32	0.02	-3.13	0.21	-0.26	0.09
	5	-12.24	-2.62	-7.60	-0.09	-4.43	0.33	-0.36	0.14
L=1.0	1			-0.07	0.00	-0.05	0.00	0.00	0.00
	2			-0.27	0.00	-0.16	0.00	-0.02	0.00
	3			-0.58	0.01	-0.35	0.00	-0.03	0.00
	4			-0.96	0.04	-0.58	0.03	-0.05	0.02
	5			-1.45	0.06	-0.87	0.05	-0.07	0.03

Note: The columns labeled .8442 use a shape factor of magnitude 0.8442. The columns labeled Matching use the shape factor found from matching the lowest natural frequency of the Timoshenko theory to the elasticity solutions for each beam geometry as indicated in Table 21.

Table 21. Shape Factor from Matching Frequencies

Beam Length (m)	Wall Thickness (m)			
	0.0005	0.001	0.002	0.004
L=0.01	0.00997	0.04718	0.234567	0.489292
L=0.02	0.019984	0.09196	0.429996	0.796788
L=0.05	0.085302	0.31106	0.512967	0.792065
L=0.1	0.264373	0.42462	0.527019	0.787272
L=0.2	0.39205	0.45690	0.529863	0.785144
L=0.4	0.43294	0.46554	0.530348	0.784297
L=1.0	--	0.46798	0.533981	0.783107

Note: These shape factors were found by iteration until the lowest natural frequency as calculated by Timoshenko theory matched the elasticity solutions

Section 5.4: Summary

- **Improved accuracy with larger slenderness ratios**
 - For slenderness ratios of at least 118.8, all three approximate beam theories are accurate to within 0.94 % for the first mode.
 - For slenderness ratios below 12.9, all three approximate beam theories show errors in excess of 96 % in most instances for the first mode.
- **Timoshenko beam theory most accurate**
 - In consideration of the error associated with all calculated natural frequencies, the Timoshenko theory provided an average improvement over the Euler-Bernoulli theory of 21.08 times, with a minimum of 1.91 times.
 - Meanwhile, it provided an average improvement of 9.58 times over the Rayleigh theory, with a minimum of 1.62 times.

- **Rayleigh theory impractical to use**
 - For slenderness ratios of at least 60.4, the Rayleigh theory is reasonably accurate, but only offers an improvement over the Euler-Bernoulli method that ranges from 0.02 % to 4.3 %.
 - In this same range, the Timoshenko theory offers improvement that ranges between 0.08 % and 30.0 %.

- **Euler-Bernoulli model accurate for very slender beams**
 - When the slenderness ratio is at least 108.2, the Euler-Bernoulli model is accurate to within 4.3 % for the first two modes of vibration.
 - With a slenderness ratio of at least 270.5, the Euler-Bernoulli theory is accurate to within 3.7 % for each of the first five modes.

- **Shape factor for hollow anisotropic beams should account for magnitude of wall thicknesses, not just their ratio, as well as the mode number**
 - In calculating natural frequencies, error can be reduced by a factor of nearly 4700 for higher order modes when matching the lowest order frequency.
 - An average improvement of 31.99 times occurs for the higher modes of vibration when utilizing this method.
 - Errors as high as 127.6 % are evident for higher order modes even after the first mode is fixed to the exact frequency, suggesting the shape factor is also dependent on the mode number.

References

- [1] Ohno, I., “Free Vibration of a Rectangular Parallelepiped Crystal and its Application to Determination of Elastic Constants of Orthorhombic Crystals”, *Journal of Physics and the Earth*, **24**, 355-379 (1976).
- [2] Benaroya, H., *Mechanical Vibration: Analysis, Uncertainties, and Control*, New Jersey: Prentice Hall, 1998.
- [3] Olhoff, N. and Parbery, R., “Optimal Structural Design for Maximum Distance Between Adjacent Eigenfrequencies”, *Lecture Notes in Control and Information Sciences*, 765-772 (1984).
- [4] Zuo, Jie., “Larger Hollow Structural Sections”, *Modern Steel Construction*, **November**, 52-54 (2011).
- [5] Traill-Nash, R. W. and Collar, A. R., “The Effects of Shear Flexibility and Rotatory Inertia on the Bending Vibrations of Beams”, *The Quarterly Journal of Mechanics and Applied Mathematics*, **6**, 186-222 (1953).
- [6] Aldraihem, O. J., Wetherhold, R. C., and Singh, T., “Intelligent Beam Structures: Timoshenko Theory vs. Euler-Bernoulli Theory”, *Proceedings of the 1996 IEEE International Conference of Control Applications*, 976-981 (1996).
- [7] Omidvar, B., “Shear Coefficient in Orthotropic Thin-Walled Composite Beams”, *Journal of Composites for Construction*, **2**, 46-56 (1998).
- [8] Kolsky, H., “The Propagation of Longitudinal Elastic Waves Along Cylindrical Bars”, *Philosophical Magazine*, **45**, 712-726 (1954).
- [9] Han, S. M., Benaroya, H., and Wei, T., “Dynamics of Transversely Vibrating Beams Using Four Engineering Beam Theories”, *Journal of Sound and Vibration*, **225**, 935-988 (1999).
- [10] Elishakoff, I. and Pentarus, D., “Apparently the First Closed-Form Solution of Inhomogeneous Elastically Restrained Vibrating Beams”, *Journal of Sound and Vibration*, **298**, 439-445 (2006).
- [11] Fung, Y. C. and Tong, P., *Classical and Computational Solid Mechanics*, **1**, New Jersey: World Scientific, 2010.
- [12] Cowper, G. R., “The Shear Coefficient in Timoshenko’s Beam Theory”, *Journal of Applied Mechanics*, **33**, 335-340 (1966).
- [13] Mindlin, R. D., “Low Frequency Vibrations of Elastic Bars”, *International Journal of Solids and Structures*, **12**, 27-49 (1976).
- [14] Rubin, M. B., “On the Quest for the Best Timoshenko Shear Coefficient”, *Journal of Applied Mechanics*, **70**, 154-157 (2003).
- [15] Puchegger, S., Loidl, D., Kromp, K., and Peterlik, H., “Hutchinson’s Shear Coefficient for Anisotropic Beams”, *Journal of Sound and Vibration*, **266**, 207-216 (2003).
- [16] Chree, C., “Longitudinal Vibrations in Solid and Hollow Cylinders”, *Proceedings of the Physical Society*, **16**, 304-322 (1897).

- [17] Benatar, A., Rittel, D., and Yarin, A. L., “Theoretical and Experimental Analysis of Longitudinal Wave Propagation in Cylindrical Viscoelastic Rods”, *Journal of the Mechanics and Physics of Solids*, **51**, 1413-1431 (2003).
- [18] Bancroft, D., “The Velocity of Longitudinal Waves in Cylindrical Bars”, *Physical Review*, **59**, 588-593 (1941).
- [19] Puckett, A. D., “A Semi-Analytical Model for Predicting Multiple Propagating Axially Symmetric Modes in Cylindrical Waveguides”, 1-33.
- [20] Abramson, H. N., Plass, H. J., and Ripperger, E. A., “Stress Wave Propagation in Rods and Beams”, *Advances in Applied Mechanics*, **5**, 111-194 (1958).
- [21] Demarest, H. H. Jr., “Cube Resonance Method to Determine the Elastic Constants of Solids”, *Journal of the Acoustical Society of America*, **49**, 768-775 (1971).
- [22] Visscher, W. M., Migliori, A., Bell, T. M., and Reinert, R. A., “On the Normal Modes of Free Vibration of Inhomogeneous and Anisotropic Elastic Objects”, *Journal of the Acoustical Society of America*, **90**, 2154-2162 (1991).
- [23] Heyliger, P. R. and Jilani, A., “The Free Vibrations of Inhomogeneous Elastic Cylinders and Spheres”, *International Journal of Solids and Structures*, **29**, 2689-2708 (1992).
- [24] Penny, J. E. and Reed, J. R., “An Integral Equation Approach to the Fundamental Frequency of Vibrating Beams”, *Journal of Sound and Vibration*, **19**, 393-400 (1971).
- [25] Schmidt, R., “Accurate Fundamental Frequencies of Vibrating Beams Via Ritz-Rayleigh-Sturm-Liouville Approach”, *Industrial Mathematics*, **39**, 37-46 (1989).
- [26] Liew, K. M. and Yang, B., “Three-Dimensional Elasticity Solutions for Free Vibrations of Circular Plates: A Polynomials-Ritz Analysis”, *Computer Methods in Applied Mechanics and Engineering*, **175**, 189-201 (1999).
- [27] Love, A. E. H., *A Treatise on the Mathematical Theory of Elasticity*, New York: Dover Publications, Inc., 287-292 (1944).
- [28] Dolph, C. L., “On the Timoshenko Theory of Transverse Beam Vibrations”, *Quarterly of Applied Mathematics*, **12**, 175-187 (1954).
- [29] Kruszewski, E. T., and Davenport, W. W., “Influence of Shear Deformation of the Cross Section on Torsional Frequencies of Box Beams”, *National Advisory Committee for Aeronautics, Technical Note 3464*, 1-23 (1955).
- [30] Huang, T. C., “The Effect of Rotatory Inertia and of Shear Deformation on the Frequency and Normal Mode Equations of Uniform Beams with Simple End Conditions”, *Journal of Applied Mechanics*, **28**, 579-584 (1961).
- [31] Thompson, R. G. and Kruszewski, E. T., “Cross-Sectional Deformations of Monocoque Beams and Their Effects on the Natural Vibration Frequencies”, *National Aeronautics and Space Administration, Technical Note D-987*, 1-45 (1961).

Appendix

Nomenclature

A	Cross-sectional area
a, b, b	Wave numbers
C_{ijkl}	Components of elastic stiffness tensor
E	Modulus of elasticity
f	Transverse force
G	Shear modulus of elasticity
I	Moment of inertia
K_{ij}	Components of stiffness matrix
k	Shape factor
k'	Radius of Gyration
L	Length of beam
M_{ij}	Components of mass matrix
m	Mass
r_i	Roots of characteristic equation, wave numbers
s	Slenderness ratio
T^n	Surface traction vector
t	Time
U	Strain energy
u, v, w, z	Displacements
$w(x, t)$	Transverse displacement
V	Volume
W	Strain energy density
KE	Kinetic energy
PE	Potential energy
ϵ	Cauchy strain
ρ	Density
σ	Cauchy stress
ω	Natural frequency
ω_c	Critical frequency
ϕ_i	Virtual displacement
ϕ_j	Function of position
ψ	Section rotation

Dimensionless Variables

$A^* = \frac{A}{L^2}$	Dimensionless area	$\omega^* = \frac{\omega t}{\omega_1}$	Dimensionless frequency
$\rho^* = \frac{\rho L^6 \omega^2}{EI}$	Dimensionless density	$I^* = \frac{I}{L^4}$	Dimensionless moment of inertia
$L^* = \frac{L}{L}$	Dimensionless length		

Table 22. Slenderness Ratios

Beam Length (m)	Wall Thickness (m)			
	0.0005	0.001	0.002	0.004
L=0.01	2.575	2.705	2.970	3.397
L=0.02	5.150	5.410	5.941	6.794
L=0.05	12.874	13.525	14.852	16.984
L=0.1	25.748	27.050	29.704	33.968
L=0.2	51.497	54.100	59.409	67.937
L=0.4	60.447	108.200	118.818	135.873
L=1.0	257.485	270.501	297.044	339.683

Cowper's Shape Factor for Thin-walled Square Tubes

$$\frac{20(1 + \nu)}{48 + 39\nu}$$

Note: ν represents the Poisson Ratio